Decomposition of available potential energy for networks of connected volumes

John Craske[1]†

[1]Department of Civil and Environmental Engineering, Imperial College London, London SW7 2AZ, UK

(Received xx; revised xx; accepted xx)

A decomposition of available potential energy is derived for Boussinesq fluid flow in networks of connected control volumes. The two constituent parts of the decomposition are positive definite and therefore meaningful representations of available energy. The first (inner) part accounts for available potential energy that is intrinsic to each control volume, while the second (outer) part accounts for the context provided by the larger parent volume to which each smaller control volume belongs. While the intended application casts the control volumes as connected rooms in a building, the formulation can be applied to any domain that is partitioned by either physical boundaries or abstract zones and can be invoked recursively to clarify the hierarchical dependence of available potential energy on scale and context. By deriving budgets for the decomposition, two ways in which available potential energy can be redistributed between its inner and outer parts are identified. The first accounts for an apparent generation of available potential energy due to diapycnal mixing within a control volume that is constrained by removable boundaries. The second involves the reversible conversion between inner and outer parts that occurs when mass or heat is transported between control volumes and accounts for the concomitant change in context. Analytical expressions are derived for the hierarchy of contributions to available potential energy in an example involving three connected spaces, before budgets for the decomposition from a direct numerical simulation are analysed. Finally, the dependence of mixing efficiency on remote regions that was identified by Davies Wykes *et al.* (2015, vol. 781, 2015, pp. 261-275) is revisited to demonstrate the precise way in which the proposed decomposition quantifies context.

1. Introduction

1.1. *Background*

Recognition by Margules (1903), Lorenz (1955) and Van Mieghem (1956) that fluids have at their disposal a limited fraction of their potential energy for conversion into kinetic energy led to the development of the concept of available potential energy (Tailleux 2013*a*). The concept has since been applied widely in atmospheric and oceanic communities, not least in focusing attention on the a priori-unknown proportion of useful energy that is extracted from stratified turbulence to produce diapycnal mixing rather than viscous dissipation, which is often discussed in terms of mixing efficiency (Linden 1979; Fernando 1991; Peltier & Caulfield 2003; Ivey *et al.* 2008; Caulfield 2020).

Available potential energy (APE) is a thermodynamic concept because it quantifies the maximum amount of useful work that can be obtained from a system (Keenan 1951; Haywood 1974; Tailleux 2013*a*) by distinguishing between different forms of energy. Like exergy (see, for example, Gaggioli 1998; Kucharski 1997), which is based on the

† Email address for correspondence: john.craske07@imperial.ac.uk

observation that convex thermodynamic potentials are minimised at equilibrium, global APE is positive definite. The relevant equilibrium (reference) state that is typically used to quantify global APE is an adiabatically rearranged density field that minimises potential energy. Like classical thermodynamics, global APE formalism developed by focusing on the energy associated with volume integrals, leading to bulk frameworks for Boussinesq (Winters *et al.* 1995) and non-Boussinesq (Tailleux 2009) fluids.

Candidates for local (pointwise) definitions of APE require careful consideration because, under volume integration, many distinct local choices map onto the same global definition of APE. Indeed, consistency can be achieved to within any function of state whose integral over the volume of interest vanishes (Winters & Barkan 2013). In this regard, Holliday & Mcintyre (1981) and Andrews (1981) derived local definitions of APE for Boussinesq and non-Boussinesq fluids, respectively, that are consistent with Lorenz (1955). These original formulations were generalised and clarified conceptually by Tailleux (2018) for multicomponent compressible stratified fluids and possess the distinguishing feature of being (locally) positive definite, making them physically meaningful and useful definitions of available energy (Roullet & Klein 2009). As described by Shepherd (1993) and Scotti & Passaggia (2019), the said functions of state are intimately related to the Casimir functions that emerge as invariants for adiabatic motion described by nonsymplectic Poisson manifolds (Littlejohn 1982; Weinstein 1983).

The use of reference states to quantify the effect of density differences is common in the analysis of buoyancy-driven flows. As described by Smith *et al.* (2005), the ability to redefine pressure allows one to define a 'local' or 'system' buoyancy, illuminating the fact that buoyancy is a derived quantity whose physical meaning depends on the context induced by the (arbitrary) choice of reference state. In their analysis of internal waves, Scotti *et al.* (2006) noted that reference states in definitions of local APE density need not correspond to an adiabatic rearrangement of the density field, while Andrews (1981) and Tailleux (2013*b*) showed that alternative reference states produce values of APE that are bounded from below by Lorenz's original (adiabatically sorted) reference state (Lorenz 1955). In relation to the analysis of local/isolated density perturbations, Lamb (2008) also considered the implications of alternative reference states in defining an APE density that features, with that of Scotti *et al.* (2006), among the alternative definitions of local APE density reviewed by Kang & Fringer (2010). More recently, issues associated with size of the domain that is used to define a reference state were addressed by Dewar & McWilliams (2019), using 'Thorpe sorting' (based on Thorpe 1977) over a vertical column to quantify the efficiency of local ocean mixing events.

In building physics the concept of APE for buoyancy-driven flows has not been applied extensively, despite the increasingly prominent role played by thermodynamical concepts such as energy storage and efficiency. Exceptions include estimations of the mechanical energy required for transition from displacement ventilation to mixing ventilation (Linden 1999; Craske & Hughes 2019) and an analysis of mixing efficiency for filling boxes (Davies Wykes *et al.* 2019). As illustrated in figure 1, a particular challenge is to reconcile the fluid dynamics of individual rooms with the behaviour of the entire building, where the latter is typically modelled as a network of connected zones (Axley 2007). Details of the flow within each zone are invisible to the network, which only accounts for the mean flow between zones that is driven by bulk pressure differences. Such treatment therefore creates a distinction between outer (large-scale) and inner (small-scale) subgrid processes, whose coupling is crucial because thermal stratification and airflow within a room affect contaminant transport, thermal comfort and advective heat transfer between adjacent rooms (see, for example, Kuesters & Woods 2012; Bhagat *et al.* 2020).

A distinguishing feature of buildings are the walls and floors that separate individual

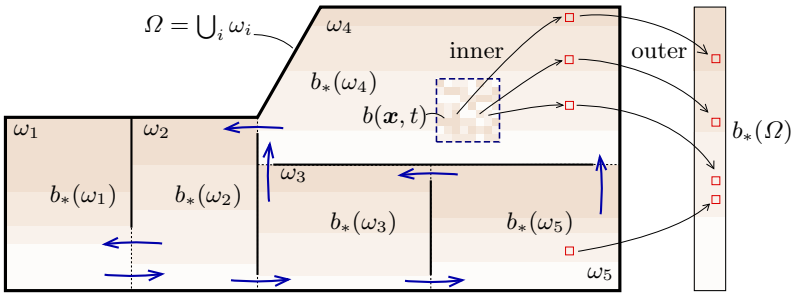


FIGURE 1. An example of the space Ω in a building as a set of connected control volumes $\omega_1, \ldots, \omega_5$ that partition Ω and are therefore subvolumes. The buoyancy within each subvolume can be adiabatically rearranged to produce reference states $b_*(\omega_1), \ldots, b_*(\omega_5)$ to minimise (and therefore release) available potential energy within each subvolume, termed 'inner' APE in §2. The reference states themselves can be rearranged globally, with respect to the larger parent volume Ω into $b_*(\Omega)$ to minimise (and therefore release) APE over the entire domain Ω, termed 'outer' APE in §2. The sum of inner and outer APE over all subvolumes $\omega_1, \ldots, \omega_5$ corresponds to the system's global APE (as defined by Winters *et al.* 1995).

rooms. Punctured by relatively small openings, such as doors and windows, the walls and floors provide constraints that make a unified understanding of a building's energetics challenging. Indeed, as noted by Andrews (2006, p. 481) in the context of momentum constraints, whilst APE sets an upper bound on the energy that can be released by reconfiguring the buoyancy field, *'in the presence of further constraints on the subsequent motion, the maximum energy available for such conversion may well be less than the APE'*, as explored in the context of topographical barriers in the ocean by Stewart *et al.* (2014). On the other hand, analysis of individual rooms is difficult because of their open nature and coupling with adjacent rooms.

To address these challenges, the aim of this work is to decompose the APE associated with individual subvolumes (rooms) of a larger volume (a building) into two parts. As labelled in figure 1, the first (inner) contribution will account for the APE that is intrinsic to a room while the second (outer) contribution will account for the APE arising from the context provided by the rest of the building. The decomposition is recursive and relies on the definition and integral properties of local APE density (Winters & Barkan 2013; Scotti & Passaggia 2019). With the application of building ventilation in mind, attention is restricted to Boussinesq fluids with a linear equation of state.

1.2. *Context matters*

Figure 2 provides simple examples of situations in which context affects the meaning and interpretation of APE. The first, shown in figure 2(a), demonstrates that the potential energy of a buoyancy field in a domain whose horizontal sections are not path connected can posses multiple local minima, as discussed by Stewart *et al.* (2014) in the context of ocean topography. In fact, example 2(a) admits infinitely many local minima, parameterised by the distance h between the buoyancy interface either side of the partition. A distinction can therefore be drawn between the potential energy that is available within each horizontally-connected subvolume and the larger potential energy that would be available if the partition were removed. Internal constraints, from boundaries such as walls or topography, provide forces found in local minima of potential energy that hold the state away from the unique global minimum. Indeed, with sufficient stirring, relatively buoyant fluid just above the density interface in ω_1 could enter ω_2

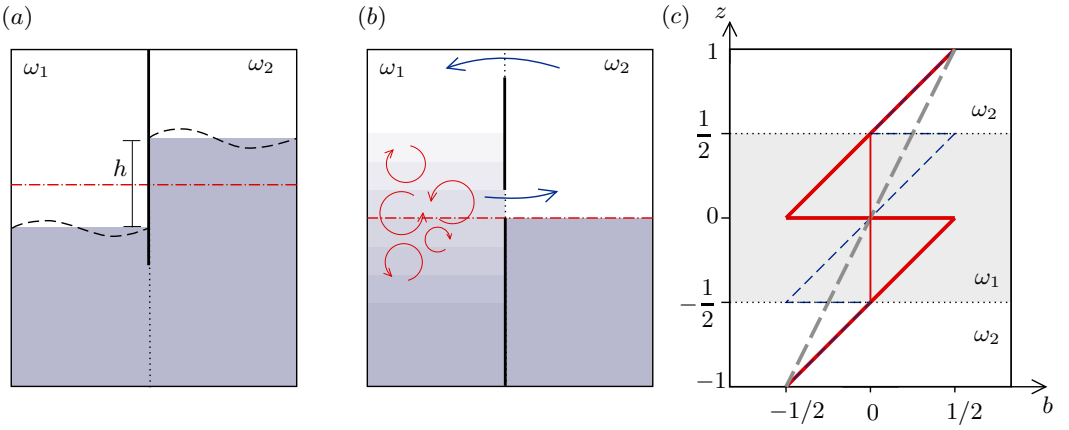


FIGURE 2. Simple examples where context is crucial in understanding the APE of subvolumes. Example (a) illustrates that the potential energy of a domain whose horizontal sections are not path connected can posses multiple local minima. In example (b) both sides of the tank initially contain a stable two-layer density profile. Irreversible diapycnal mixing of ω_1, enhanced by stirring, gives ω_1 a higher centre of mass than ω_2, which would lead to counter-clockwise circulation between the tanks if openings were added in the partition. Example (c) is from Davies Wykes *et al.* (2015), who considered mixing of the (unstably-) stratified fluid in region ω_1 (thick red line) to produce a uniform buoyancy (thin red line). Here, APE depends on whether ω_1 is considered in isolation or as part of $\Omega = \omega_1 \cup \omega_2$, in spite of the fact that the APE associated with ω_2 is zero because its initial distribution of buoyancy is also its reference state. However, the individual reference states for ω_1 and ω_2 (thin dashed blue line) possess available potential energy with respect to the global reference state over Ω (thick dashed grey line).

and therefore tap into a global reservoir of available potential energy that would not be apparent from the sum of APE that is intrinsic to each subvolume. In §2 the APE that is intrinsic to a given subvolume is referred to as 'inner' APE and the difference between a local minimum of potential energy and the global state of minimum potential energy is attributed to 'outer' APE, as suggested in figure 1.

The example in figure 2(b) shows that irreversible diapycnal mixing can appear to create APE when subvolumes are separated by a physical partition. If ω_1 and ω_2 initially contain the same two-layer stable stratification then the system resides in a (unique) state of global minimum potential energy. However, stirring of the fluid in ω_1 to enhance mixing will eventually result in ω_1 having a higher centre of mass than ω_2, leaving the system's potential energy in a local, but not global, minimum. Available potential energy can be subsequently released, by making openings in the partition, to bring the system closer to the state of global minimum potential energy. In §4.1 budgets for the decomposition described in §2 are derived to quantify the effect that diapycnal mixing has on the inner and outer parts of a system's APE.

The final example of a situation in which context matters is from Davies Wykes *et al.* (2015), who considered the unstable profile of buoyancy shown in figure 2(c), prior to the homogenisation of ω_1. Context is relevant in this example because the hypothetical mixing of fluid in ω_1 need not involve fluid from ω_2. Yet, the 'mixing efficiency' of the process, defined as the increase in background potential energy divided by the initial available potential energy, depends on whether the calculation is based on ω_1 or $\Omega = \omega_1 \cup \omega_2$. As shown in figure 2($c$), the reason is that the reference state for ω_1 does not coincide with the reference state for Ω. Indeed, the reference state of ω_1 (when ω_2 is ignored) possesses available potential energy with respect to Ω. Consequently, Davies Wykes *et al.* (2015, p. 273) remark that *'a mixing efficiency that is independent of the volume of interest can*

be defined only if that volume is at least as large as the region affected by an adiabatic rearrangement of the initial density field to a statically stable state', which is a stringent condition of reducibility that complicated systems are unlikely to satisfy. This example is revisited in §6.1, after APE is decomposed into inner and outer parts in §2 to quantify the precise role that context plays in complicated systems.

1.3. *Outline*

In §2 the proposed decomposition is described. Starting with existing local definitions of available potential energy density in §2.1, inner and outer contributions to the APE of subvolumes are defined in §2.2. In §3 an example involving three subvolumes is discussed, for which all parts of the APE decomposition can be deduced analytically. In §4 budgets for the APE decomposition are derived and two mechanisms responsible for conversion between inner and outer APE are identified. To complement and extend §3, §5 considers the time evolution of the APE budget using data from a two-dimensional direct numerical simulation. In §6 the implications of the results are discussed by revisiting figure 2(c) in §6.1 and the recursive properties of the decomposition are summarised in §6.2.

2. Inner and outer available potential energy (APE)

Before accounting for context in defining the APE of a subvolume in §2.2, this section reviews the motivation behind the local (pointwise) definition of local APE density, developed originally by Holliday & Mcintyre (1981) for a Boussinesq fluid with a linear equation of state and shown by Winters & Barkan (2013) to be equivalent to the widely applied bulk formulation of APE for Boussinesq fluids described by Winters *et al.* (1995).

2.1. *Local APE density*

To quantify the portion of a flow's potential energy that is available to perform 'useful' work, it is necessary to define a reference state that minimises potential energy. Such a construction is analogous to reference states of minimum internal energy or maximum entropy in thermodynamics. The reference state is found from a volume-preserving and adiabatic rearrangement of the buoyancy field into a state that is in stable hydrostatic equilibrium. As discussed in §1.2, if all horizontal sections of the domain are path connected (cf. figure 2(a), which shows a domain whose horizontal sections are not path connected), then the reference state is unique. Under the rearrangement, a parcel of fluid at location $\boldsymbol{x} = (x, y, z)$ with buoyancy $b(\boldsymbol{x})$ is mapped to the vertical position $z_*(b(\boldsymbol{x}))$ and the rearranged buoyancy field is denoted b_*, which means that $b_*(z_*(b)) = b$.

The APE $A(\Omega)$ associated with a buoyancy field in a domain Ω accounts for the potential energy $(z_* - z)b$ associated with displacing each parcel of fluid from the (unique) reference equilibrium state of minimum potential energy that was described in the preceding paragraph (Winters *et al.* 1995), and is therefore positive definite,

$$A(\Omega) = \int_\Omega (z_* - z) b \, \mathrm{d}V \geqslant 0. \tag{2.1}$$

By definition, the minimum value of zero in (2.1) is produced by the reference field itself, for which $b = b_*$ and $z_* = z$.

Pointwise, however, $(z_* - z)b$ is not positive definite because b does not necessarily have the same sign as $(z_* - z)$ (Roullet & Klein 2009). But, inclusion of the energy associated with the rearrangement of the reference state that would accompany the movement of a

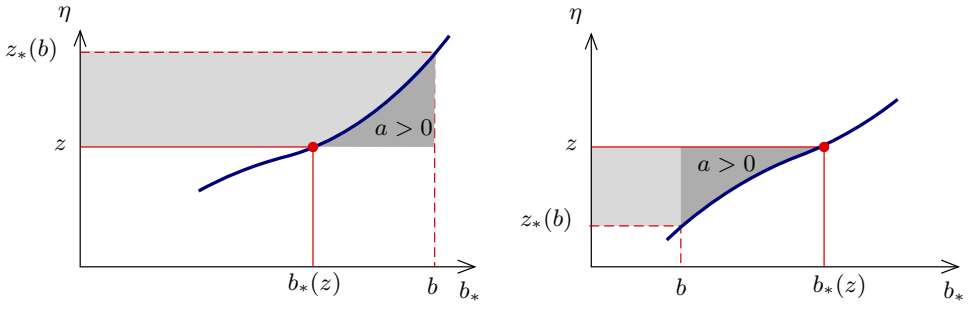


FIGURE 3. Geometric 'proof' that (2.2) is positive definite when b_* is a monotonically increasing function with $b_*(z_*) = b$. The left-hand axis illustrates a case for which $b_*(z) < b$ (and therefore $z < z_*(b)$) and the right-hand axis illustrates a case for which $b < b_*(z)$ (and therefore $z_*(b) < z$).

single parcel from z_* to z, leads to

$$a = (z_* - z)b - \underbrace{\int_z^{z_*} b_*(\eta)d\eta}_{a_*}, \tag{2.2}$$

which, as illustrated in figure 3, is positive definite if b_* is monotonic and $b_*(z_*) = b$ (Holliday & Mcintyre 1981; Scotti *et al.* 2006), and is therefore a viable thermodynamic quantity analogous to exergy (Tailleux 2013*a*). For a detailed discussion about how (2.2) emerges from a gauge-fixing condition in terms of Casimir functions (invariants), the reader is referred to Scotti & Passaggia (2019). Conversely, the local available potential energy (2.2) can be regarded as the Legendre transform of a_* (which is convex because b_* increases monotonically) if z_* is regarded as a free parameter, such that

$$a = \max_{z_*} \{(z_* - z)b - a_*\}, \tag{2.3}$$

and the maximising condition that $b_*(z_*) = \mathrm{d}a_*/\mathrm{d}z_* = b$ emerges naturally as the 'force' that is conjugate to the displacement $z_* - z$ releasing the maximum potential energy.

As noted by Tailleux (2013*a*), the thermodynamic nature of APE in (2.2) is not obvious from the integral definition (2.1) because, since the operation leading to z_* is a volume preserving and adiabatic rearrangement of fluid in the domain,

$$\int_\Omega \int_{\xi(z)}^{\xi(z_*)} g(\eta)\,\mathrm{d}\eta\,\mathrm{d}V = 0, \tag{2.4}$$

for any functions g and ξ; hence the volume integral of a_* (for which g corresponds to b_* and ξ corresponds to the identity function) over Ω vanishes. To understand why, it is useful to regard z_* as a permutation of fluid parcels of finite volume, which can be decomposed into a finite number of cycles (see e.g. MacLane & Birkhoff 1999). Using a suitable change of variables to account for ξ, the integral of $g(\eta)$ over each cycle vanishes because it can be decomposed into an integral over $[z, z_*]$ followed by an integral over $[z_*, z]$, which necessarily cancel because integrals of g, which depend only on the vertical coordinate, are path independent. Winters & Barkan (2013) provide a more detailed explanation for the particular case corresponding to a_* in (2.2) and Scotti & Passaggia (2019) provide a more general explanation in terms of the symmetry associated with the system's Casimir functions.

To account for (2.4), which plays a fundamental role in the decomposition described in §2.2, an equivalence relation (see, for example MacLane & Birkhoff 1999), denoted $\overset{\Omega}{\cong}$, can be defined for expressions whose difference vanishes upon integration over a given domain Ω. For example, application of (2.4) to (2.2) allows us to write

$$a \overset{\Omega}{\cong} (z_* - z)b, \tag{2.5}$$

to express the equality of a and $b(z_* - z)$ to within terms whose integral over Ω is zero.

2.2. *The APE of subvolumes*

The construction of APE described in §2.1 involves a reference state computed from the buoyancy field in Ω. However, if the volume Ω is partitioned into subvolumes $\omega_i \subset \Omega$, then each subvolume has its own reference state $b_*(\omega_i)$ corresponding to the rearrangement of the buoyancy field within ω_i to minimise the potential energy of ω_i, as illustrated in figure 1. Together, the reference states of each subvolume have a potential energy that is at least as large as the unconstrained reference state associated with the parent volume Ω. Consequently, the sum of each subvolume's APE will be less than, or at best equal to, the maximum energy that can be released through reconfiguration of the buoyancy field over Ω. In such cases, the physical or notional boundaries that separate the subvolumes provide 'forces' that are conjugate to the additional displacements that would be required to release the full APE over Ω.

Starting from (2.2), consider the local APE in a subvolume $\omega \subset \Omega$ with respect to the reference state of the parent volume Ω,

$$a(\Omega) = \big[z_*(\Omega) - z\big]\, b - \int_z^{z_*(\Omega)} b_*(\Omega)|_\eta \,\mathrm{d}\eta. \tag{2.6}$$

To be explicit, and to avoid subscripts, the notation $z_*(\Omega)$, $b_*(\Omega)$ will be used to define the functions that map a buoyancy b to the vertical position $z_*(\Omega)|_b$ and a height z to the corresponding reference buoyancy $b_*(\Omega)|_z$, respectively. The notation '$|\cdot$' (such as $|_\eta$, $|_b$ and $|_z$ above) should be read as '*evaluated at* $\cdot$', but will be omitted for brevity when arguments to functions are clear from the context.

Following the examples in §1.2, it is useful to account separately for the APE of fluid within ω relative to: (i) the parent reference height $z_*(\Omega)$ and (ii) the subvolume reference height $z_*(\omega)$. Specifically, it is useful to represent the available energy released during a two-stage sorting process $z \mapsto z_*(\omega) \mapsto z_*(\Omega)$, in which a parcel of fluid is moved to its equilibrium position in ω, before being moved to its final equilibrium position in Ω. To express the decomposition mathematically, (2.6) can be refactored as

$$a(\Omega) = \underbrace{\big[z_*(\Omega) - z_*(\omega)\big]\, b}_{(i)} + \underbrace{\big[z_*(\omega) - z\big]\, b}_{(ii)} - \int_z^{z_*(\Omega)} b_*(\Omega)|_\eta \,\mathrm{d}\eta. \tag{2.7}$$

But (2.7) is unsatisfactory, because terms (i) and (ii) are not individually positive definite and the integral of b_* is composite, involving both $z \mapsto z_*(\omega)$ and $z_*(\omega) \mapsto z_*(\Omega)$. However, (2.4) can be used to reformulate (2.7) by adding and subtracting terms that vanish upon integration over the subvolume ω, enabling the integral of b_* in (2.7) to be appropriately distributed between terms (i) and (ii).

Although the reference state $b_*(\Omega)$ is not necessarily the same as $b_*(\omega)$, (2.4) usefully implies that the net work associated with rearranging $b_*(\Omega)$ over ω is zero, modulo

integration over ω (cf. Scotti *et al.* 2006; Scotti & Passaggia 2019), such that

$$\int_{z}^{z_*(\omega)} b_*(\Omega)|_\eta \,\mathrm{d}\eta \overset{\omega}{\cong} 0. \tag{2.8}$$

The physical meaning of the decomposition (2.7) is therefore made explicit by invoking (2.8) to repartition the contributions to (i) and (ii),

$$a(\Omega) \overset{\omega}{\cong} \underbrace{[z_*(\Omega) - z_*(\omega)]\, b - \overbrace{\int_{z_*(\omega)}^{z_*(\Omega)} b_*(\Omega)|_\eta \,\mathrm{d}\eta}^{a_*(\Omega|\omega)}}_{a(\Omega|\omega)\geqslant 0} + \underbrace{[z_*(\omega) - z]\, b - \overbrace{\int_{z}^{z_*(\omega)} b_*(\omega)|_\eta \,\mathrm{d}\eta}^{a_*(\omega)\overset{\omega}{\cong}0}}_{a(\omega)\geqslant 0}. \tag{2.9}$$

The contribution $a(\omega)$ corresponds to the APE inside the subvolume ω without reference to the context provided by Ω. In contrast, the contribution $a(\Omega|\omega)$ corresponds to the additional potential energy of fluid within ω that can be made available by removing the partitions of Ω. Both contributions are positive definite because they have the same form as (2.2) and will therefore play a crucial role in accounting for context in §4.3, with regards to the transport of APE between subvolumes. Although the right-hand side of (2.9) does not correspond to the traditional definition of APE density (2.6) in a pointwise sense, it articulates the two-stage sorting process and is equivalent to (2.6) under integration over the subvolume ω. The decomposition (2.9) appears to be similar to the mean/eddy decomposition of APE density for a compressible fluid described by Tailleux (2018, §4.1) to account for 'non-resting' reference states (cf. Andrews 2006). A notable difference, however, is that (2.9) was able to make use of (2.8) to remove sign-indefinite contributions, modulo integration over ω.

Integration of (2.9) provides a decomposition for the APE of ω, given Ω, whose constituent parts add together to give the integral of the traditional local APE density defined in (2.6),

$$A(\omega|\Omega) = \underbrace{\int_{\omega} a(\Omega|\omega)\,\mathrm{d}V}_{A(\Omega|\omega)\geqslant 0} + \underbrace{\int_{\omega} a(\omega)\,\mathrm{d}V}_{A(\omega)\geqslant 0} = \int_{\omega} a(\Omega)\,\mathrm{d}V. \tag{2.10}$$

For the reasons stated below (2.9), $A(\Omega|\omega)$ is referred to as 'outer' APE and $A(\omega)$ is referred to as 'inner' APE. The total APE $A(\omega|\Omega)$ associated with ω is the sum of its inner and outer parts (for $A(\omega|\Omega)$ read '*the APE of* ω *given* Ω' and for $A(\Omega|\omega)$ read '*the APE of* Ω *given* ω'). The outer APE $A(\Omega|\omega)$ corresponds to the positive energy required to create the subvolume reference state $b_*(\omega)$ by rearranging the global/parent reference state $b_*(\Omega)$, while the inner APE $A(\omega)$ corresponds to the positive energy required to create the buoyancy field b by rearranging the subvolume reference state $b_*(\omega)$ over ω. For mathematical readers, the choice of terminology comes from noting that, for a Boussinesq fluid, an adiabatic rearrangement of the buoyancy field is a permutation and that permutations leaving the contents of each subvolume unchanged can be regarded as subgroups (cf. the closed-loop cycles in §4 of Winters & Barkan 2013). In this way the outer APE involves permutations that belong to the quotient of Ω-permutations with the (inner) ω-permutations, which is reminiscent of the relationship between inner and outer automorphisms from group theory (cf. MacLane & Birkhoff 1999).

The (global) APE $A(\Omega)$ of the parent domain Ω is obtained by summing (2.10) over

all subvolumes ω belonging to a partition $\mathcal{P}(\Omega)$ of Ω,

$$A(\Omega) = \sum_{\omega\in\mathcal{P}(\Omega)} A(\Omega|\omega) + \sum_{\omega\in\mathcal{P}(\Omega)} A(\omega). \tag{2.11}$$

In figure 1, for example, $\mathcal{P}(\Omega) = \{\omega_1, \omega_2, \omega_3, \omega_4, \omega_5\}$. If $A(\Omega) = 0$, then $A(\Omega|\omega) = 0$ and $A(\omega) = 0$ for all $\omega \subset \Omega$ because $A(\Omega|\omega)$ and $A(\omega)$ are positive definite. Application of (2.4) shows that the combined contribution from the integrals of $a_*(\Omega|\omega)$ within $A(\Omega|\omega)$ over each subvolume vanishes in (2.11) because, in summation, the integrals of $a_*(\Omega|\omega)$ over ω correspond to an integral over Ω,

$$\sum_{\omega\in\mathcal{P}(\Omega)} A(\Omega|\omega) = \sum_{\omega\in\mathcal{P}(\Omega)} \int_\omega [z_*(\Omega) - z_*(\omega)]\, b \,\mathrm{d}V - \underbrace{\sum_{\omega\in\mathcal{P}(\Omega)} \int_\omega \overbrace{\int_{z_*(\omega)}^{z_*(\Omega)} b_*(\Omega)|_\eta \,\mathrm{d}\eta}^{a_*(\Omega|\omega)} \,\mathrm{d}V}_{0}. \tag{2.12}$$

which shows that (2.11) is equivalent to the global APE (2.1). As explained in §6.2, (2.11) can be applied recursively to subsets of Ω down to infinitesimal subvolumes (i.e. individual points $\boldsymbol{x}$), for which the inner APE $A(\boldsymbol{x})$ necessarily vanishes and the outer APE $A(\omega|\boldsymbol{x})$ corresponds to the local APE density (2.6) with respect to ω.

2.3. *Background potential energy*

The background potential energy (BPE) associated with a buoyancy field in Ω is the potential energy of the reference state $b_*(\Omega)$. The BPE is therefore equal to the difference between the system's potential energy and the global APE $A(\Omega)$. As described in §2.2 for APE, the BPE of a particular subvolume $\omega \subset \Omega$ can be split between outer and inner contributions that do and do not make reference to the context provided by Ω, respectively. Formally, the definitions follow from subtracting the right-hand side of (2.9) from the potential energy $-bz$ and integrating over the subvolume ω,

$$B(\omega|\Omega) = -A(\omega|\Omega) - \int_\omega bz \,\mathrm{d}V = \underbrace{-A(\Omega|\omega)}_{B(\Omega|\omega)} \underbrace{- \int_\omega bz_*(\omega) \,\mathrm{d}V}_{B(\omega)}. \tag{2.13}$$

The inner BPE $B(\omega)$ accounts for the subvolume reference state $b_*(\omega)$, while the outer BPE $B(\Omega|\omega)$ accounts for the eventual position of the reference state $b_*(\omega)$ within the parent volume Ω. The outer components of BPE are necessarily equal in magnitude and opposite in sign to the outer components of APE $A(\Omega|\omega)$, which means that $B(\Omega|\omega) \leqslant 0$; hence

$$B(\Omega) = \sum_{\omega\in\mathcal{P}(\Omega)} B(\Omega|\omega) + \sum_{\omega\in\mathcal{P}(\Omega)} B(\omega) \leqslant \sum_{\omega\in\mathcal{P}(\Omega)} B(\omega). \tag{2.14}$$

Equation (2.14) implies that the sum of the inner background potential energy in each subvolume is bounded from below by the global background potential energy $B(\Omega)$, which corresponds to the fact that $b_*(\Omega)$ is the global minimiser of potential energy. More generally, the inner BPE is subadditive under the union of any subsets of Ω,

$$B(\omega_1 \cup \omega_2) \leqslant B(\omega_1) + B(\omega_2), \tag{2.15}$$

which implies, and is implied by, the inner APE being superadditive under the union of

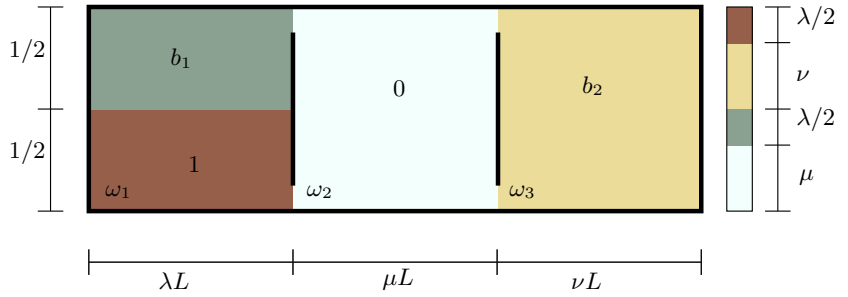


FIGURE 4. The arrangement of connected volumes $\Omega = \omega_1 \cup \omega_2 \cup \omega_3$, whose power set $\mathcal{T}(\Omega) = \{\varnothing, \omega_1, \omega_2, \omega_3, \omega_1 \cup \omega_2, \omega_2 \cup \omega_3, \omega_3 \cup \omega_1, \Omega\}$, is displayed in the Hasse diagram in figure 5. The length of Ω is L (i.e. $\lambda + \mu + \nu = 1$) and the bar on the right corresponds to the global reference state $b_*(\Omega)$ when $0 \leqslant b_1 \leqslant b_2 \leqslant 1$.

any subsets of Ω,

$$A(\omega_1 \cup \omega_2) \geqslant A(\omega_1) + A(\omega_2), \tag{2.16}$$

as observed in possible formulations of APE in the presence of topographical barriers by Stewart *et al.* (2014). Any gap between the left- and right-hand sides of (2.16) results from the potential energy that can be made available by joining ω_1 and ω_2 and is a direct consequence of the positivity of the outer APE $A(\Omega|\omega_1)$ and $A(\Omega|\omega_2)$.

In providing a lower bound on the APE $A(\omega_1 \cup \omega_2)$, (2.16) resembles the result obtained by Andrews (1981), and explained by Tailleux (2013*b*), that the APE defined with respect to alternative reference states is bounded from below by the APE corresponding to the unique (Lorenz) reference state obtained from an adiabatic transformation of the buoyancy field. As seen in (2.15), the reason for the resemblance is that constraints on the reference state increase background potential energy and therefore reduce available potential energy. The difference, however, is that in (2.15) and (2.16) the constraint comes from the isolation of subvolumes, rather than the adiabatic constraint embodied by the Lorenz reference state.

3. Analytical example

In this section the ideas outlined in §2.2 are clarified using the simple example illustrated in figure 4. The domain Ω consists of three 'rooms': ω_1, ω_2 and ω_3. High- and low-level openings connect ω_1 to ω_2 and ω_2 to ω_3. If the upper and lower halves of ω_1 contain fluid of buoyancy $b_1 \leqslant 1$ and 1, respectively, and the volumes ω_2 and ω_3 contain fluid of uniform buoyancy 0 and b_2, respectively, how do the geometrical parameters λ, μ and ν affect the constitution of the system's initial APE?

In this example, the set of subsets (or power set) of Ω is $\mathcal{T}(\Omega) = \{\varnothing, \omega_1, \omega_2, \omega_3, \omega_1 \cup \omega_2, \omega_2 \cup \omega_3, \omega_3 \cup \omega_1, \Omega\}$. As depicted in the Hasse diagram of figure 5, $\mathcal{T}(\Omega)$ is a partially ordered set under the operation of inclusion (e.g. $\omega_1 \subset \omega_1 \cup \omega_2$). Each node of the Hasse diagram represents the inner APE of that volume and an arrow from a set $X \in \mathcal{T}$ to a set $Y \in \mathcal{T}$, where $X \subset Y$, represents the outer available potential energy $A(Y|X)$ of X with respect to Y. The bottom of the diagram represents all (empty) infinitesimal points $\boldsymbol{x}$, whose inner APE is necessarily zero. The nodes and arrows of the Hasse diagram therefore represent all possible APEs that one might wish to define and provides a graphical interpretation of the various subvolume APEs that can be combined according to (2.11). For example, the global APE $A(\Omega)$ can be decomposed into inner

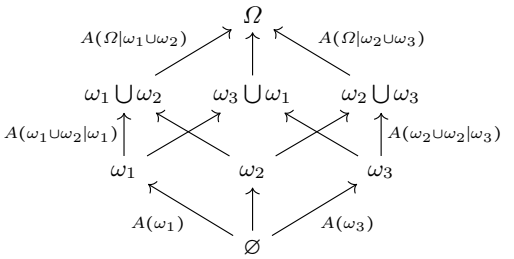


FIGURE 5. The Hasse diagram of the partially ordered power set $\mathcal{T}(\Omega)$ corresponding to all combinations of the rooms in figure 4. An arrow from a set $X \in \mathcal{T}$ to a set $Y \in \mathcal{T}$, where $X \subset Y$, represents the outer APE $A(Y|X)$ that characterises the context provided by Y for X. Each node of the diagram represents the inner APE associated with a given set (i.e. subvolume), which can be decomposed into various different components by following the arrows and nodes downwards. The bottom of the diagram represents infinitesimal points as empty sets, which have zero inner APE, as discussed further in §6.2.

and outer components for each subvolume in the partition $\mathcal{P}(\Omega) = \{\omega_1 \cup \omega_2, \omega_3\}$,

$$A(\Omega) = \underbrace{A(\Omega|\omega_1 \cup \omega_2) + A(\omega_1 \cup \omega_2)}_{A(\omega_1 \cup \omega_2|\Omega)} + \underbrace{A(\Omega|\omega_3) + A(\omega_3)}_{A(\omega_3|\Omega)}. \tag{3.1}$$

All components of the APE associated with figures 4 and 5 can be calculated analytically and are enumerated explicitly in appendix A for cases in which $0 \leqslant b_1 \leqslant b_2 \leqslant 1$. As indicated in table 1 (appendix A), some of the contributions can be deduced from others by applying the relationships established in §2.2 recursively.

Figure 6 displays the value of several APE components with respect to the subvolume width parameters λ, μ and ν. For generality, and to avoid having to make assumptions about the relative size of 0, b_1, b_2 and 1, the data plotted in figure 6 were generated numerically. The algorithm employs a one-dimensional discretisation of the reference states over the 'finest' partition $\{\omega_1, \omega_2, \omega_3\}$ of Ω. In this way the outer APE associated with joining subvolumes was calculated recursively by sorting concatenated reference states and verified against the analytical expressions listed in appendix A.

In figure 6(a) the relative width λ of volume ω_1 is regarded as variable and $\mu = 1/3$ is fixed, with $\nu = 2/3 - \lambda$, $b_1 = 1/2$ and $b_2 = 3/4$. When $\lambda = 0$, ω_1 does not contribute APE, and figure 6(a) shows that the total APE in the system is equal to $A(\omega_2 \cup \omega_3)$. As λ increases, the system's global APE $A(\Omega)$ increases. The increase is primarily because the growth of the inner APE $A(\omega_1)$, and the outer APE $A(\Omega|\omega_1)$, associated with ω_1 exceeds the reduction in APE associated with $\omega_2 \cup \omega_3$. The fact that the outer APE $A(\Omega|\omega_1)$ accounts for a significant fraction of the APE associated with ω_1 illustrates that the context provided by ω_2 and ω_3 is important. As illustrated on the right-hand side of figure 4, the sorting process over Ω splits ω_1 because $b_1 \leqslant b_2 \leqslant 1$, releasing APE that is not included in $A(\omega_1)$.

In figure 6(b) the width ν and buoyancy b_2 of volume ω_3 are regarded as variable, with $\lambda = 1/3$, $b_1 = 1/2$ and the APE $A(\omega_2 \cup \omega_3) = 1/16$ held constant. As seen at the edges of the shaded regions (where $1 < b_2$), when $\nu = 1/6$ or $\nu = 1/2$, $b_2 = 1$ and the global reference state changes discontinuously. When $\nu = 1/2$ the global APE $A(\Omega)$ is minimised. As ν increases from 0, the global APE $A(\Omega)$ is dominated by the reduction in the size of $\omega_1 \cup \omega_2$, because the outer contribution $A(\Omega|\omega_1 \cup \omega_2)$ is insignificant when $b_1 \leqslant b_2 \leqslant 1$. When $1 < b_2$, however, the outer contribution $A(\Omega|\omega_1 \cup \omega_2)$ becomes significant. To see why, assume that $\mu \approx 0$ and note that when $b_1 \leqslant b_2 \leqslant 1$ the centre of mass of ω_3 does not

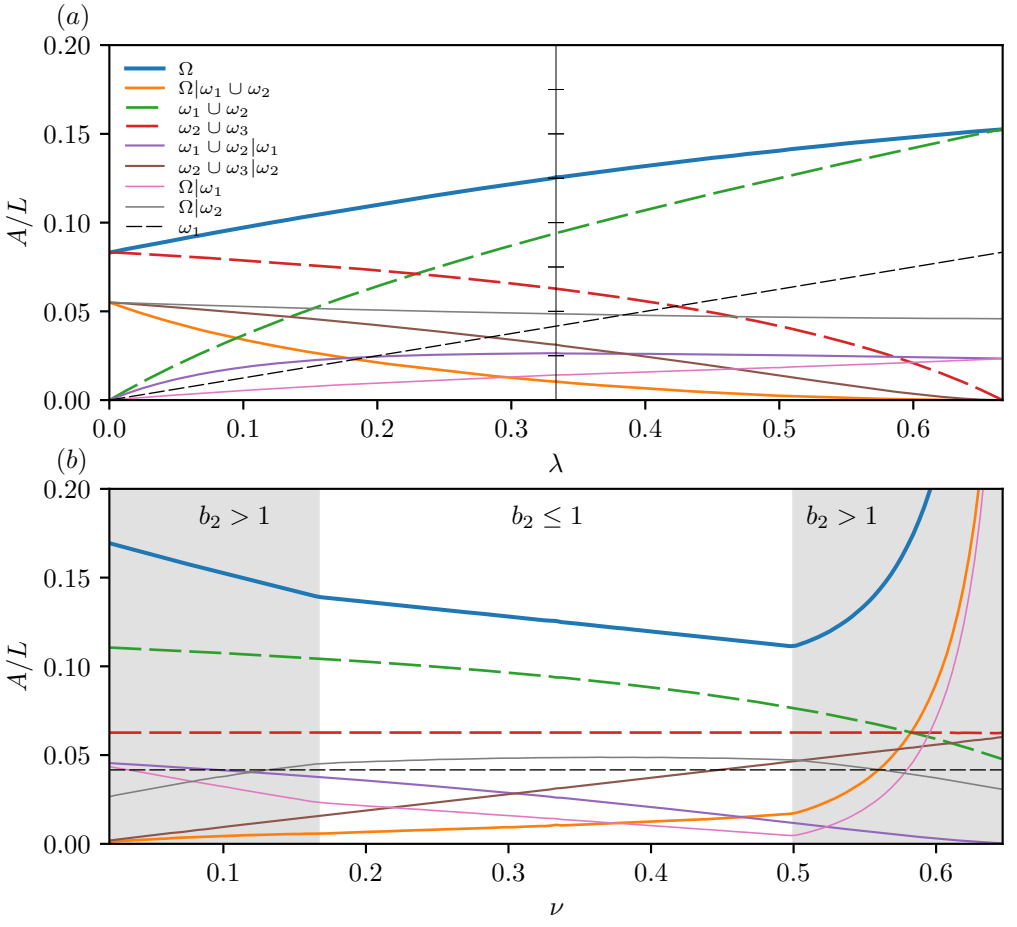


FIGURE 6. Components of the APE associated with figure 4. Panel (a) displays the effect of changing the relative width λ of volume ω_1 without changing $\mu = 1/3$ such that $\nu = 2/3 - \lambda$ with $b_1 = 1/2$ and $b_2 = 3/4$. Panel (b) displays the effect of changing the relative width ν and buoyancy b_2 of subvolume ω_3 without changing the APE $A(\omega_2 \cup \omega_3) = 1/16$ and $\lambda = 1/3$ with $b_1 = 1/2$. The vertical line in the centre of panel (a) is placed at $\lambda = 1/3$ for comparison with §5.

change when it is sorted with respect to $\omega_1 \cup \omega_2$, but when $1 < b_2$ available energy can be released through placement of ω_3 at the top of Ω. In the example shown in figure 6(b) the global APE $A(\Omega)$ increases without bound as $\nu \to 2/3$ because $b_2 \to \infty$ in order to maintain the constraint $A(\omega_2 \cup \omega_3) = 1/16$.

4. Inner and outer APE budgets

The non-dimensionalised equations of motion for Boussinesq fluid flow are

$$\frac{\partial \boldsymbol{u}}{\partial t} + \boldsymbol{u} \cdot \nabla \boldsymbol{u} = -\nabla p + b\,\boldsymbol{k} + \frac{1}{Re}\nabla^2 \boldsymbol{u}, \tag{4.1}$$

$$\nabla \cdot \boldsymbol{u} = 0, \tag{4.2}$$

$$\frac{\partial b}{\partial t} + \boldsymbol{u} \cdot \nabla b = \frac{1}{Pe}\nabla^2 b, \tag{4.3}$$

where $\boldsymbol{u}$ is the velocity, p is the kinematic pressure, $\boldsymbol{k}$ is the unit vector in the vertical (z) direction and Re and Pe are Reynolds and Péclet numbers, respectively.

4.1. *Budgets for inner and outer APE*

Using (4.1)-(4.3) and the relation (2.4), the budget for the inner APE $A(\omega)$ is obtained by applying $\mathrm{d}/\mathrm{d}t$ and ∇^2 to the local APE,

$$a(\omega) = [z_*(\omega) - z]\, b - \int_z^{z_*(\omega)} b_*(\omega)|_\eta \,\mathrm{d}\eta, \tag{4.4}$$

defined relative to the subvolume ω, and integrating over ω (see, for example, Scotti & White 2014),

$$\begin{aligned}\frac{\mathrm{d}A(\omega)}{\mathrm{d}t} = &- Y(\omega) - \overbrace{\int_\omega \int_b^{b_*(\omega)} \frac{\partial z_*(\omega)}{\partial t}\bigg|_\beta \mathrm{d}\beta\,\mathrm{d}V}^{T(\omega)=0} + \overbrace{\int_\omega w\,[b_*(\omega) - b]\,\mathrm{d}V}^{C(\omega)} \\ &\underbrace{- \frac{1}{Pe}\int_\omega |\nabla b|^2 \frac{\partial z_*(\omega)}{\partial b} - \frac{\partial b_*(\omega)}{\partial z}\,\mathrm{d}V}_{D(\omega)} \underbrace{- \frac{2}{Pe}\int_\omega \left[\frac{\partial b_*(\omega)}{\partial z} - \frac{\partial b}{\partial z}\right]\mathrm{d}V}_{2L(\omega)},\end{aligned} \tag{4.5}$$

where

$$Y(\omega) = \int_{\partial\omega} \left(\boldsymbol{u} - \frac{\nabla}{Pe}\right) a(\omega)\cdot\boldsymbol{n}\,\mathrm{d}s, \tag{4.6}$$

accounts for 'transport' across the subvolume boundary $\partial\omega$ (relative to which the unit normal $\boldsymbol{n}$ points outwards) and will be discussed in §4.3. As shown by Scotti & Passaggia (2019, §2), the integral contribution in (4.5) from temporal changes in the background state, $T(\omega)$, vanishes (to see why, replace ξ with b_* and g with $\partial_t z_*$ in (2.4), which expresses the fact that ω-integrated functionals of the reference state are not affected by the adiabatic sorting $z \mapsto z_*(\omega)$). Equation (4.5) is equivalent to the global budgets discussed in Winters *et al.* (1995), who considered closed domains (such that $\boldsymbol{u} = 0$ on $\partial\omega$) and factored the linear terms in $Y(\omega)$, $D(\omega)$ and $2L(\omega)$ slightly differently.

Following the definition in (2.10) of local APE relative to Ω, replacement of ω with Ω in (4.5) (except in specifying the domain of integration ω) yields an equivalent expression for the budget of the total (outer plus inner) APE $A(\omega|\Omega) = A(\Omega|\omega) + A(\omega)$. The budget of the outer APE $A(\Omega|\omega)$ therefore corresponds to the difference between the budget of the total APE and the inner APE,

$$\begin{aligned}\frac{\mathrm{d}A(\Omega|\omega)}{\mathrm{d}t} = &- \sum Y(\Omega|\omega) - \overbrace{\int_\omega \int_{b_*(\omega)}^{b_*(\Omega)} \frac{\partial z_*(\Omega)}{\partial t}\bigg|_\beta \mathrm{d}\beta\,\mathrm{d}V}^{T(\Omega|\omega)} + \overbrace{\int_\omega w[b_*(\Omega) - b_*(\omega)]\,\mathrm{d}V}^{C(\Omega|\omega)} \\ &\underbrace{- \frac{1}{Pe}\int_\omega |\nabla b|^2 \left[\frac{\partial z_*(\Omega)}{\partial b} - \frac{\partial z_*(\omega)}{\partial b}\right] - \left[\frac{\partial b_*(\Omega)}{\partial z} - \frac{\partial b_*(\omega)}{\partial z}\right]\mathrm{d}V}_{D(\Omega|\omega)} \\ &\underbrace{- \frac{2}{Pe}\int_\omega \left[\frac{\partial b_*(\Omega)}{\partial z} - \frac{\partial b_*(\omega)}{\partial z}\right]\mathrm{d}V}_{2L(\Omega|\omega)},\end{aligned} \tag{4.7}$$

where

$$Y(\Omega|\omega) = \int_{\partial\omega} \left(\boldsymbol{u} - \frac{\nabla}{Pe}\right) a(\Omega|\omega) \cdot \boldsymbol{n}\, \mathrm{d}s. \tag{4.8}$$

Equation (4.7), unlike (4.5), contains a contribution from temporal changes in the reference state $T(\Omega|\omega)$ that does not vanish upon integration over ω because it makes reference to the context provided by Ω.

4.2. *Conversion between inner and outer APE due to mixing*

The total dissipation $D(\omega|\Omega)$ of available potential energy within subvolume $\omega \subset \Omega$ is

$$D(\omega|\Omega) = D(\Omega|\omega) + D(\omega) = \frac{1}{Pe} \int_{\omega} |\nabla b|^2 \frac{\partial z_*(\Omega)}{\partial b} - \frac{\partial b_*(\Omega)}{\partial z}\, \mathrm{d}V, \tag{4.9}$$

which is equivalent to the integral of G_p in Scotti & White (2014). At the global minimum in potential energy the total dissipation $D(\omega|\Omega)$, along with its outer and inner components $D(\Omega|\omega)$ and $D(\omega)$, respectively, vanishes for each subvolume ω because, when $A(\Omega) = 0$, $\partial_z b = \partial_z b_*(\Omega)$ everywhere. However, the same cannot be said about a local minimum in potential energy (cf. figure 2(*a*)), for which $\partial_z b = \partial_z b_*(\omega) \neq \partial_z b_*(\Omega)$ in general.

With the exception of somewhat pathological cases, constructed by squeezing part of a reference state b_* horizontally to obtain a local buoyancy field b that satisfies $|\nabla b| = \partial_z b < \partial_z b_*$, the inner dissipation $D(\omega)$ and the total dissipation $D(\omega|\Omega)$ are typically positive. In contrast, the sign of the outer component of the APE 'dissipation',

$$D(\Omega|\omega) = \frac{1}{Pe} \int_{\omega} |\nabla b|^2 \left[\frac{\partial z_*(\Omega)}{\partial b} - \frac{\partial z_*(\omega)}{\partial b}\right] - \left[\frac{\partial b_*(\Omega)}{\partial z} - \frac{\partial b_*(\omega)}{\partial z}\right] \mathrm{d}V, \tag{4.10}$$

depends on the reference state of both ω and Ω. Because $|\nabla b|^2 \geqslant 0$, stirring will generally make the first term in the integrand of (4.10) dominant, such that the sign of $\partial_b z_*(\Omega) - \partial_b z_*(\omega)$ determines the sign of $D(\Omega|\omega)$. In figure 2(*b*), for example, stirring that leads to mixing of the fluid in the left subvolume ω_1 would raise the background potential energy associated with the reference state $z_*(\omega_1)$ such that $\partial_b z_*(\Omega) - \partial_b z_*(\omega_1) < 0$ and $D(\Omega|\omega) < 0$. Stirring (followed by mixing) would therefore result in the conversion of inner APE $A(\omega_1)$ to outer APE $A(\Omega|\omega_1)$. The physical explanation relates to the constraint provided by the solid partition, which enables part of the 'irreversible' work $D(\omega|\Omega)$ to be stored as outer (context dependent) APE $A(\Omega|\omega_1)$ that can be subsequently released by connecting ω_1 and ω_2.

In summary, the context that Ω provides to a subvolume ω is crucial in determining the effect that irreversible mixing within ω has on the subvolume's outer APE. This is noteworthy because, as will be seen in §5, outer APE is primarily responsible for driving flow between subvolumes separated by physical partitions. It is therefore useful to regard $D(\Omega|\omega)$ as a conversion between inner and outer APE, as shown schematically on the left-hand side of figure 7. In the following section another mechanism for conversion between inner and outer APE is described.

4.3. *Conversion between inner and outer APE due to transport*

The terms $Y(\omega)$ and $Y(\Omega|\omega)$ defined in (4.6) and (4.8), respectively, need to be considered carefully because, since they do not involve the APE of adjacent subvolumes,

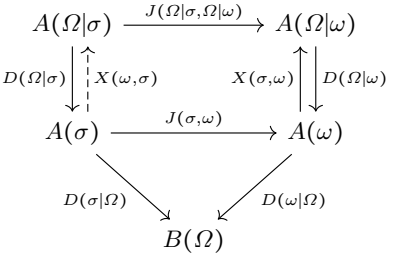


FIGURE 7. Diagram illustrating two ways in which inner APE can be converted into outer APE. The first, $D(\Omega|\omega)$, is discussed in §4.2 and accounts for diapycnal mixing that increases the outer APE at the expense of inner APE in example 2(b). The second, $X(\sigma,\omega)$, accounts for the change in context that occurs when fluxes $J(\Omega|\sigma,\Omega|\omega)$ and $J(\sigma,\omega)$ transport heat or mass from σ into ω. The conversion $X(\omega,\sigma)$ is dashed because if all pointwise fluxes from σ to ω are positive then $X(\omega,\sigma)=0$, as described in the paragraph below (4.12). An example of X can be found in the large-scale circulation driven by outer APE that is discussed in §5 (see figure 8), whose transport of buoyancy creates (or removes) inner APE from individual subvolumes.

they are not proper transport terms. Instead, it desirable to define transport terms that can account for APE transported into ω from an adjacent subvolume σ.

On the boundary between ω and σ the inner and outer APE densities $a(\omega)$, $a(\sigma)$, $a(\Omega|\omega)$ and $a(\Omega|\sigma)$ that feature in (4.6) and (4.8) are not the same, because ω and σ provide different local contexts. However, the local potential energy $-zb$ and the local APE density $a(\Omega)$ (i.e. with respect to the parent volume Ω) in (2.9) have a single value anywhere in Ω, which makes it possible to isolate those parts of $Y(\omega)$ and $Y(\Omega|\omega)$ that correspond to transport.

The definition of local APE density $a(\omega)$ in (2.9) in terms of $a(\sigma)$ at a point on the boundary $\partial\omega$ between ω and σ, noting that the potential energy $-zb$ is uniquely defined on $\partial\omega$, is

$$a(\omega) = a(\sigma) + \underbrace{\big[z_*(\omega) - z_*(\sigma)\big]\, b + a_*(\sigma) - a_*(\omega)}_{\Delta(\sigma,\omega)}, \tag{4.11}$$

which enables $Y(\omega)$ to be expressed as the sum of a flux J and a conversion term X,

$$Y(\omega) = \underbrace{\int_{\partial\omega} \left(\boldsymbol{u} - \frac{\nabla}{Pe}\right) a(\theta)\cdot\boldsymbol{n}\,\mathrm{d}s}_{\sum_{\sigma\in\mathcal{P}(\Omega)} -J(\sigma,\omega)} + \underbrace{\int_{\partial\omega} \left(\boldsymbol{u} - \frac{\nabla}{Pe}\right) \Delta(\theta,\omega)\cdot\boldsymbol{n}\,\mathrm{d}s}_{\sum_{\sigma\in\mathcal{P}(\Omega)} X(\sigma,\omega)}, \tag{4.12}$$

where θ, which depends on $\boldsymbol{u}$ and position on the boundary $\partial\omega$, is the subvolume from which $\boldsymbol{u}$ points outwards (for definiteness, this description focuses on cases for which $Pe \gg 1$ and therefore ignores the direction associated with $-\nabla a$). Transport $J(\sigma,\omega)$ corresponds to the flux of inner APE density from any subvolume $\sigma \in \mathcal{P}(\Omega)$ into $\omega \in \mathcal{P}(\Omega)$, and is skew-symmetric such that $J(\sigma,\omega) = -J(\omega,\sigma)$. Therefore, over parts of the boundary $\partial\omega$ where $\theta \neq \omega$ in (4.12), $J(\sigma,\omega) > 0$ is a flux into ω, while in cases where $\theta = \omega$, $J(\sigma,\omega) = -J(\omega,\sigma) < 0$ is a flux out of ω (under the assumption that $Pe \gg 1$). If ω is not connected to σ then $J(\sigma,\omega) = 0$ because the subvolume σ will not feature in the integral of fluxes over $\partial\omega$. Alongside J, X accounts for the change in context that occurs when APE is transported into ω from σ. Unlike J, X is not skew-symmetric because fluxes into ω from σ (i.e. $\theta = \sigma$) contribute to $X(\sigma,\omega)$ but do not contribute to $X(\omega,\sigma)$.

Since the local APE density,

$$a(\Omega) = a(\Omega|\omega) + a(\omega) = a(\Omega|\sigma) + a(\sigma), \tag{4.13}$$

is uniquely defined at boundaries, the conversion terms $X(\sigma,\omega)$ in (4.12) appear with opposite sign in the expression for $Y(\Omega|\omega)$,

$$Y(\Omega|\omega) = Y(\omega|\Omega) - Y(\omega) = \underbrace{\int_{\partial\omega} \left(\boldsymbol{u} - \frac{\nabla}{Pe}\right) a(\Omega|\theta)\cdot\boldsymbol{n}\,\mathrm{d}s - \sum_{\sigma\in\mathcal{P}(\Omega)} X(\sigma,\omega)}_{\sum_{\sigma\in\mathcal{P}(\Omega)} -J(\Omega|\sigma,\Omega|\omega)}. \tag{4.14}$$

When fluid (or thermal energy) is transported into a subvolume, the conversion term X repartitions the inner and outer APE to account for the new context. For example, the transport of fluid from a subvolume σ with uniform buoyancy, and therefore zero inner APE ($A(\sigma) = 0$), can produce inner APE ($A(\omega) > 0$) in an adjacent subvolume of different buoyancy, at the expense of a reduction in the outer APE $A(\sigma\cup\omega|\omega)$. The decomposition therefore quantifies the effect that transport across the boundary of an open system (i.e. a subvolume) has on its relationship with the surrounding environment. The role of X is illustrated schematically alongside the effects of mixing that were discussed in §4.2 in figure 7. The resulting budgets from (4.5) and (4.7) are

$$\frac{\mathrm{d}A(\omega)}{\mathrm{d}t} = C(\omega) + \overbrace{D(\Omega|\omega) - D(\omega|\Omega)}^{-D(\omega)} - 2L(\omega) + \sum_{\sigma\in\mathcal{P}(\Omega)} \left[J(\sigma,\omega) - X(\sigma,\omega)\right], \tag{4.15}$$

$$\frac{\mathrm{d}A(\Omega|\omega)}{\mathrm{d}t} = C(\Omega|\omega) - D(\Omega|\omega) - 2L(\Omega|\omega) - T(\Omega|\omega) + \sum_{\sigma\in\mathcal{P}(\Omega)} \left[J(\Omega|\sigma,\Omega|\omega) + X(\sigma,\omega)\right]. \tag{4.16}$$

5. Numerical example

In this section the APE decomposition (2.10) is applied to the Navier-Stokes equations (4.1)-(4.3), which are approximated on a two-dimensional domain described by coordinates (x,z). The use of a two-dimensional domain is computationally convenient in providing a relatively simple example that illustrates the ideas introduced in §2 and §4 transparently and without loss of generality. For simplicity, the buoyancy field was sorted directly to obtain reference states, rather than by adopting the more efficient approach described by Tseng & Ferziger (2001) using probability density functions.

The configuration is based on figure 4 with $L = 3$, $\gamma = \mu = \nu = 1/3$, $b_1 = 1/2$ and $b_2 = 3/4$. The length and time scales used to non-dimensionalise (4.1)-(4.3) are the height of the domain and the maximum initial buoyancy, as shown in figure 4. The Reynolds and Péclet numbers are $Re = 20\,000$ and $Pe = 20\,000$, respectively.

The code used to solve (4.1)-(4.3) is a two-dimensional second-order version of the fourth-order finite volume code described in Craske & van Reeuwijk (2015). To represent the non-dimensionalised domain of size 3×1 (see figure 4) a uniform grid of 2304×768 cells is used. The vertical walls separating the subvolumes ω_1, ω_2 and ω_3 are two cells thick and implemented with an immersed boundary method. Neumann boundary conditions $\boldsymbol{n}\cdot\nabla b = 0$ on buoyancy, where $\boldsymbol{n}$ is the outward wall-normal direction, are imposed at all solid boundaries and, in conjunction with the central differencing used on the

domain's interior, implemented such that buoyancy is conserved to machine precision. No-slip conditions $\boldsymbol{u} = \mathbf{0}$ are imposed on the velocity field at all solid boundaries. Time integration is performed using a second-order Adams-Bashforth scheme with an adaptive step size. Running the simulation for 20 non-dimensional time units takes approximately 2 hours on one core of an Intel Xeon E5-2690 v4 2.60GHz CPU.

5.1. *Buoyancy field evolution*

Figure 8 displays the buoyancy field at different times during the simulation. The positive buoyancy of fluid in ω_1 and ω_3, relative to ω_2, leads to counter-rotating circulation around each partition (clockwise over $\omega_1 \cup \omega_2$ and counter-clockwise over $\omega_2 \cup \omega_3$). The initial configuration of buoyancy within ω_1, which is unstable, is not the same as it is in ω_3, destroying the symmetry implied by the average buoyancy of each subvolume (equal to $3/4$ in ω_1 and ω_3). Regions of mixing are indicated by blue ($b \approx 0.25$) and yellow ($b \approx 0.75$). By $t = 10$ the structure of the initial large scale circulations and transport between subvolumes is less pronounced and has been replaced with vigorous mixing within each subvolume.

Figure 9 displays histograms corresponding to the probability density functions for buoyancy in ω_1, ω_2 and ω_3, in which $V_*(\omega_i)(b)$ is the volume of ω_i below $z_*(\omega_i)(b)$. At $t = 0$, the distribution of buoyancy consists of spikes at $b = 1/2$ and $b = 1$ for ω_1, $b = 0$ for ω_2 and $b = 3/4$ for ω_3. Panels corresponding to later times illustrate that the distribution of buoyancy within each subvolume gets wider as the system evolves because diapycnal mixing creates intermediate values of buoyancy that were not present in the initial distributions. For example, panels (f)-(l) show that an increasing proportion of fluid in ω_3 has buoyancy $b \approx 3/8 = 0.375$ due to transport of fluid with $b \approx 0$ from ω_2 into ω_1. The particular evolution of the subvolume buoyancy distributions therefore depends on the system's topology.

The probability densities shown in figure 9 are crucial in modulating the local and global dissipation of available potential energy that results from diapycnal mixing. In (4.5) the dissipation $D(\omega)$ of inner APE accounts for the distribution of buoyancy within ω (i.e. $\partial_b z_*(\omega)$) in product with the dissipation of buoyancy variance $|\nabla b|^2/Pe$. In (4.7), however, the dissipation $D(\Omega|\omega)$ of outer APE necessarily accounts for the context provided by Ω via the global reference distribution $\partial_b z_*(\Omega)$.

5.2. *APE evolution*

Figure 10 displays the temporal evolution of the APE decomposition in each subvolume. For reference, the global APE $A(\Omega) = A(\omega_1 \cup \omega_2 \cup \omega_3)$ divided by three is shaded. Dashed lines, which correspond to the total APE $A(\omega|\Omega)$ for each subvolume and therefore sum to $A(\Omega)$, indicate whether the total APE of a given subvolume is above or below the average for Ω. As can be deduced analytically (see the tabulated expressions in appendix A), at $t = 0$, $A(\omega_1) = 1/8$, $A(\omega_2) = 0$, $A(\omega_3) = 0$, $A(\Omega|\omega_1) = 1/24$, $A(\Omega|\omega_2) = 7/48$ and $A(\Omega|\omega_3) = 3/48$; hence (at $t = 0$),

$$A(\Omega) = \sum A(\Omega|\omega_i) + \sum A(\omega_i) = \frac{1}{8} + \frac{1}{24} + \frac{7}{48} + \frac{3}{48} = \frac{3}{8}. \tag{5.1}$$

In ω_1 the initial inner APE $A(\omega_1) = 1/8$ is significantly larger than the initial outer APE $A(\Omega|\omega_1) = 1/24$, and both contributions diminish as the system evolves. In contrast, the inner APE $A(\omega_2)$ and $A(\omega_3)$, which are initially zero, increase due to the transport of buoyancy between volumes, and the conversion between outer and inner APE (described by X in §4.3), which will be discussed further in §5.3. In this regard, the outer APE decays more rapidly than the inner APE because the outer APE drives the large-scale

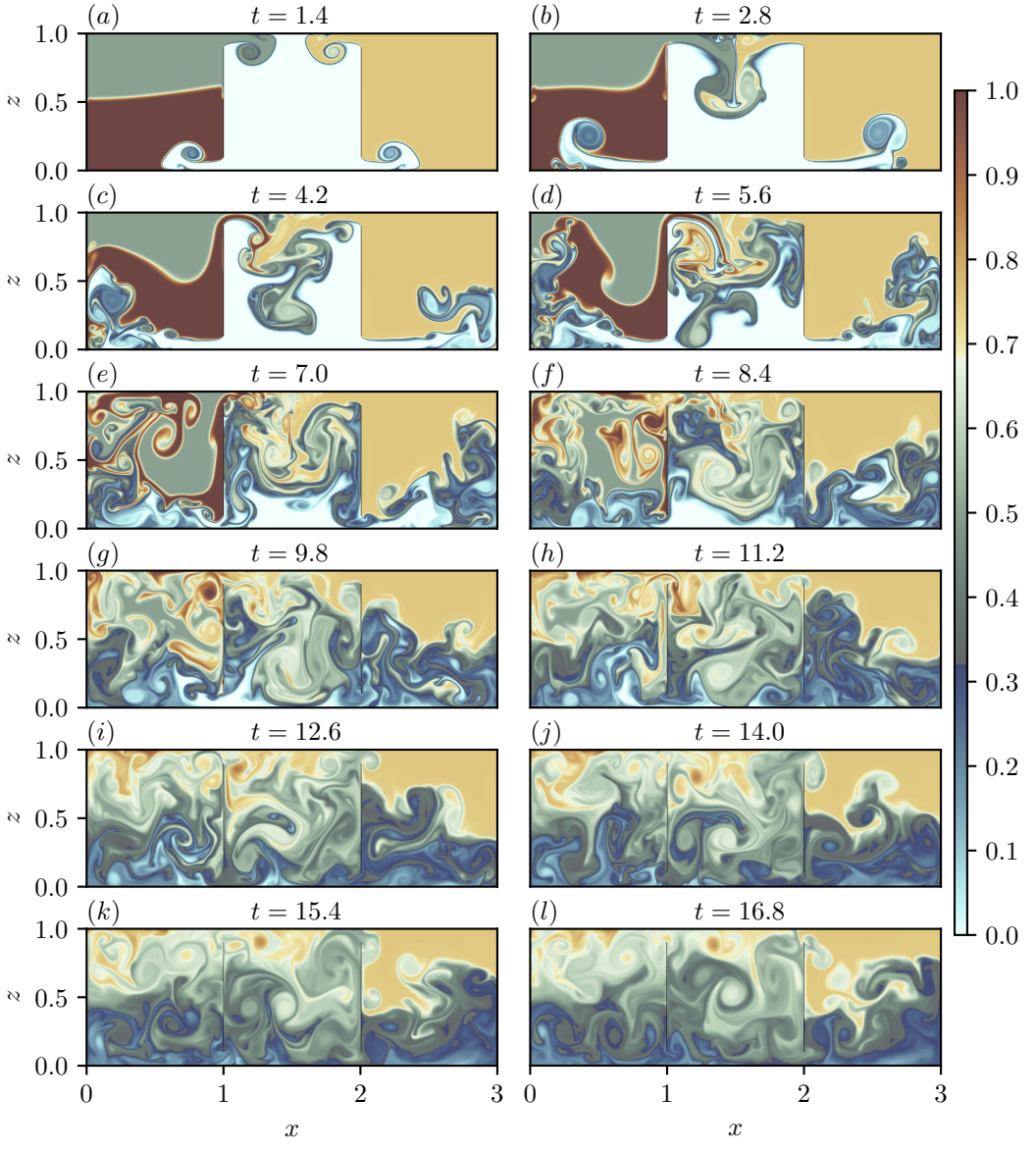


FIGURE 8. The instantaneous buoyancy field from the numerical simulation described in §5 and figure 4 with geometrical parameters $L = 3$ and $\gamma = \mu = \nu = 1/3$, and initial conditions $b_1 = 1/2$ and $b_2 = 3/4$. The colour map is from '3 Wave Colormaps' at 'https://sciviscolor.org' and was selected to highlight regions of mixing around $b = 0.25$ and $b = 0.75$ in blue and yellow, respectively (see, for example Samsel *et al.* 2019).

circulation between subvolumes that is ultimately responsible for generating inner APE in ω_2 and ω_3. After approximately 5 time units the sum of inner APE $\sum A(\omega_i)$ dominates the sum of outer APE $\sum A(\Omega|\omega_i)$, which marks the onset of significant stirring followed by mixing within each subvolume, as can be seen qualitatively in panels (d)-(l) of figure 8.

The largest contribution to the outer APE comes from $A(\Omega|\omega_2)$, due to the context provided by ω_1 and ω_3. Indeed, at $t = 0$, $A(\Omega|\omega_2)$ is comparable to the total APE

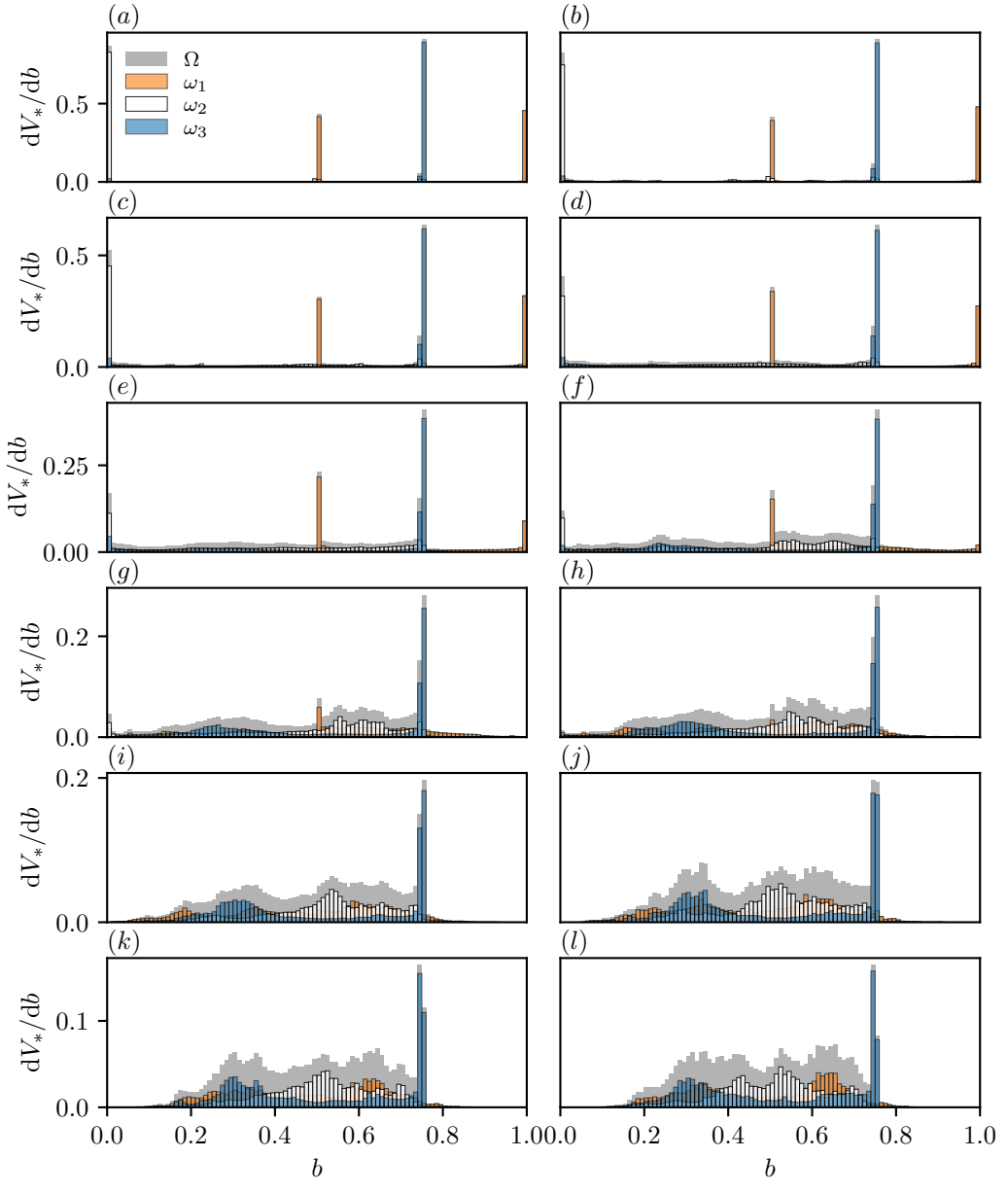


FIGURE 9. Probability density functions for the buoyancy field shown in each panel of figure 8 in each subvolume. Note that the histograms corresponding to ω_1, ω_2 and ω_3 represent probability densities because the subvolumes, unlike their sum Ω, have unit volume. Also note that the scale used on the vertical axes is different in each row of the figure.

$A(\Omega|\omega_1) + A(\omega_1)$ of ω_1, in spite of the fact that $b \equiv 0$ in ω_2. At around $t = 10$, the total APE in ω_2, which becomes dominated by the inner APE $A(\omega_2)$, is larger than the inner APE in ω_1.

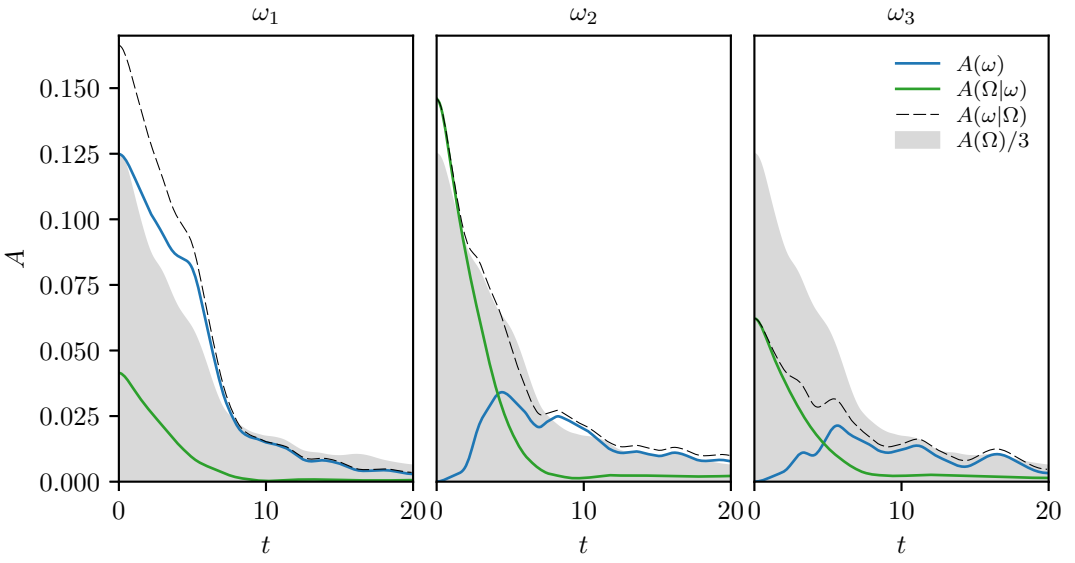


FIGURE 10. The temporal evolution of outer APE $A(\Omega|\omega)$, inner APE $A(\omega)$ and their sum $A(\omega|\Omega)$ for subvolumes ω_1, ω_2 and ω_3. The shaded region corresponds to $A(\Omega)/3$ and therefore represents the volume-averaged global APE to which contributions within each subvolume can be compared.

5.3. *Subvolume APE budgets*

Figure 11 displays each term of the inner APE budget (4.15) with respect to time. Due to the flow's high Reynolds and Péclet number, diffusion down the inner reference states $L(\omega)$ is relatively small. For the same reason, the diffusive contribution to the transport terms J and X is excluded, which makes their calculation significantly simpler and their physical meaning more transparent. The residual numerical error shown in figure 11 is relatively small, which implies that (4.15) has been derived and implemented correctly. The error is not identically zero because pointwise contributions to the APE dissipation $D(\omega)$, which involves the product of three gradients, from the small number of computational cells that are adjacent to the corners of the solid boundaries between subvolumes are difficult to calculate accurately (see, for example, figure 13 for a picture of the local APE dissipation).

In each subvolume the dissipation of inner APE $D(\omega)$ reaches a maximum after approximately 8 units of time. During the first 4 units of time the transport $J(\omega_2,\omega_1) < 0$ (which is the only term contributing to $\sum J$) corresponds to the inner APE that is lost from ω_1 as relatively dense (unstable) parcels of fluid are transported out of the volume at high level and replaced with relative dense (stable) parcels of fluid at low level. This effect provides an example of how outer APE can drive flows that reduce inner APE within a subvolume. The loss of inner APE in ω_1 due to $J(\omega_2,\omega_1) < 0$ corresponds exactly to the gain in inner APE in ω_2 due to $J(\omega_1,\omega_2) > 0$, which justifies regarding J, defined in (4.12), as transport. However, the parcels of fluid with initial buoyancy b_1, which were negatively buoyant in ω_1, become stable at the top of ω_2. This change in context is quantified by $-X(\omega_1,\omega_2)$ in (4.12), which corresponds to a conversion from the inner APE $A(\omega_2)$ into the outer APE $A(\Omega|\omega_2)$, and therefore appears as a sink in figure 11(b).

The most significant remaining term in figure 11 is the buoyancy work C, defined relative to the reference state of each subvolume, which represents the well-known

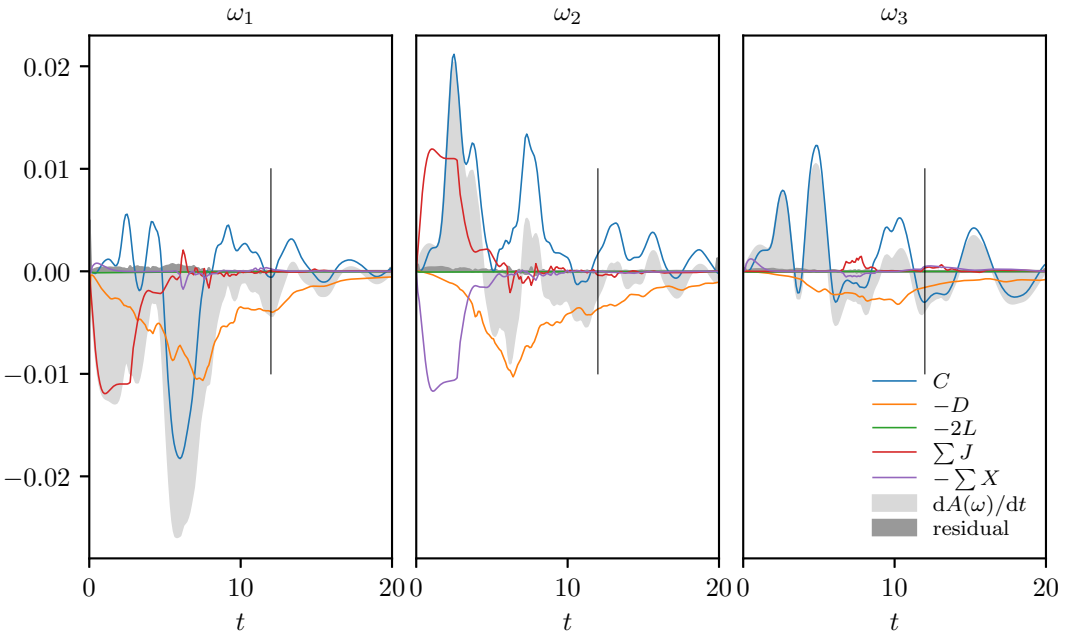


FIGURE 11. Terms in the budget of inner APE (4.15) for each subvolume (for the definitions of individual terms see (4.5) and (4.12)). The light grey shaded region corresponds to the temporal derivative of inner APE and the dark shaded region corresponds to the residual numerical error that is left when the terms in (4.15) are added together. The vertical line corresponds to the upper limit of the time domain used in figure 12.

reversible conversion between APE and kinetic energy. Its relatively large negative contribution in ω_1 at $t \approx 6$ corresponds to the instability within ω_1 arising from the unstable initial buoyancy state. In contrast, $C(\omega_2)$ is typically positive, due to circulation within ω_2 that transports relatively buoyant fluid entering ω_2 at high level downwards and lifts relatively dense fluid upwards (see, for example, panel (e) in figure 8).

Figure 12 displays the temporal evolution of terms in the outer APE budget (4.16). The dominant term in all subvolumes is the (outer) conversion $C(\Omega|\omega)$. In contrast to $C(\omega)$, which accounts for ω without context, $C(\Omega|\omega)$ accounts for work over the reference buoyancy field and can only be non-zero when there is a mean vertical motion in a subvolume (because neither $b_*(\Omega)$ nor $b_*(\omega)$ in (4.7) depend on x), resulting from high- and low-level openings in this particular problem. Consequently, figure 12 shows that outer APE is lost in each subvolume, because $C(\Omega|\omega)$ is negative, to drive the large-scale circulation between subvolumes.

A further noteworthy feature of figure 12(b) is the positive contribution from $X(\omega_1, \omega_2)$ (cf. $-X(\omega_1, \omega_2)$ in figure 11(b)), which corresponds to the (reversible) conversion between inner and outer APE due to transport between subvolumes, as discussed above in relation to figure 11; the advection of parcels of fluid that are unstable with respect to ω_1, but stable with respect to ω_2, effectively converts inner APE $A(\omega_1)$ into outer APE $A(\Omega|\omega_2)$ via transport $J(\omega_1, \omega_2)$, in accordance with figure 7.

5.4. *Local APE dissipation*

Figure 13(a) displays the local inner APE dissipation, whose integral over each subvolume is $D(\omega)$, as defined in (4.5). As can be seen from the colour scale used in figure

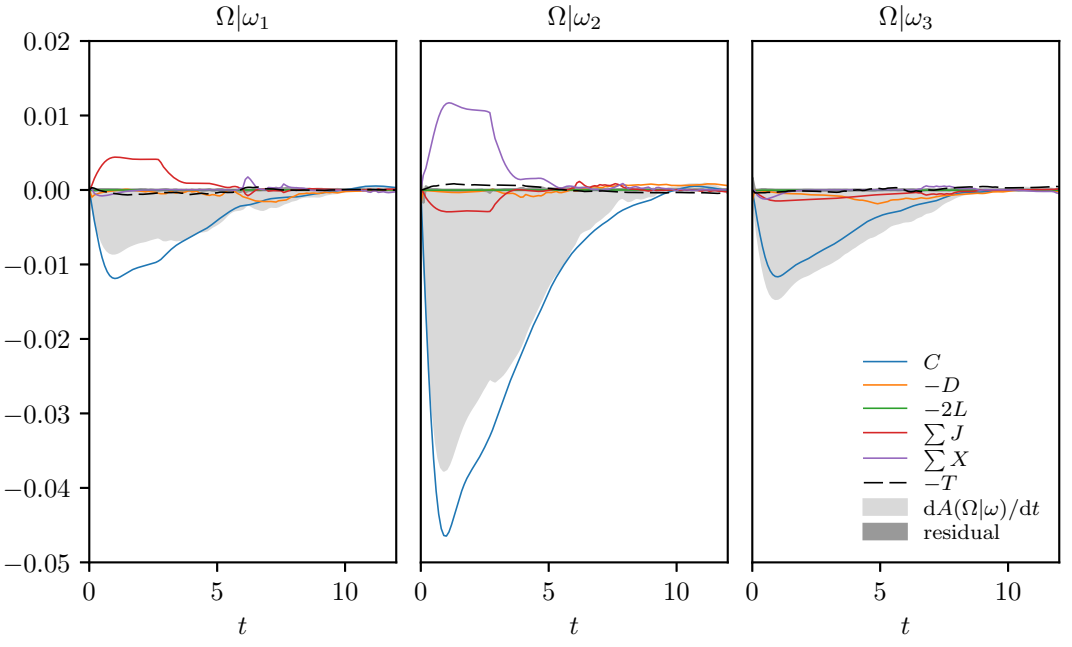


FIGURE 12. Terms in the budget of outer APE (4.16) for each subvolume (for the definitions of individual terms see (4.7), (4.12) and (4.14)). The light grey shaded region corresponds to the temporal derivative of outer APE and the dark shaded region corresponds to the residual numerical error that is left when the terms in (4.16) are added together. Note that D corresponds to the outer dissipation $D(\Omega|\omega) = D(\omega|\Omega) - D(\omega)$ in (4.16) and that X corresponds to $\sum X(\sigma, \omega)$ in (4.16), and therefore appears in this figure with a sign that opposite to the $-X$ that appears in figure 11.

13(a), APE dissipation is dominated by large contributions from thin filaments, where both $|\nabla b|$ and $\partial z_*/\partial b$ are large.

As discussed in §4.2, although the inner and total APE dissipation ($D(\omega)$ and $D(\omega|\Omega)$, respectively) are typically positive, the sign of the 'dissipation' associated with the outer APE, $D(\Omega|\omega) = D(\omega|\Omega) - D(\omega)$, depends on context. Indeed, figure 13(b), which displays local contributions to the outer APE dissipation $D(\Omega|\omega)$, highlights positive and negative contributions that correspond to a loss or gain of outer APE, respectively, due to local mixing. In this particular problem, for which figure 12 indicates that the integral $D(\Omega|\omega)$ is small for all ω, the positive and negative contributions appear to occur in approximately equal proportion within each subvolume.

6. Discussion

In §6.1, the example shown in figure 2(c) of §1.2 is revisited from the perspective of the decomposition developed in §2 and §4, and in §6.2 the recursive properties of the decomposition are discussed.

6.1. *Context matters (revisited)*

As discussed in Davies Wykes *et al.* (2015), the underlying difficulty associated with the example shown in figure 2(c) is that the reference state computed from the contents of ω_1 is not the same as the reference state computed from the contents of Ω. The decomposition described in §2 quantifies the role of context by identifying outer $A(\Omega|\omega_1)$

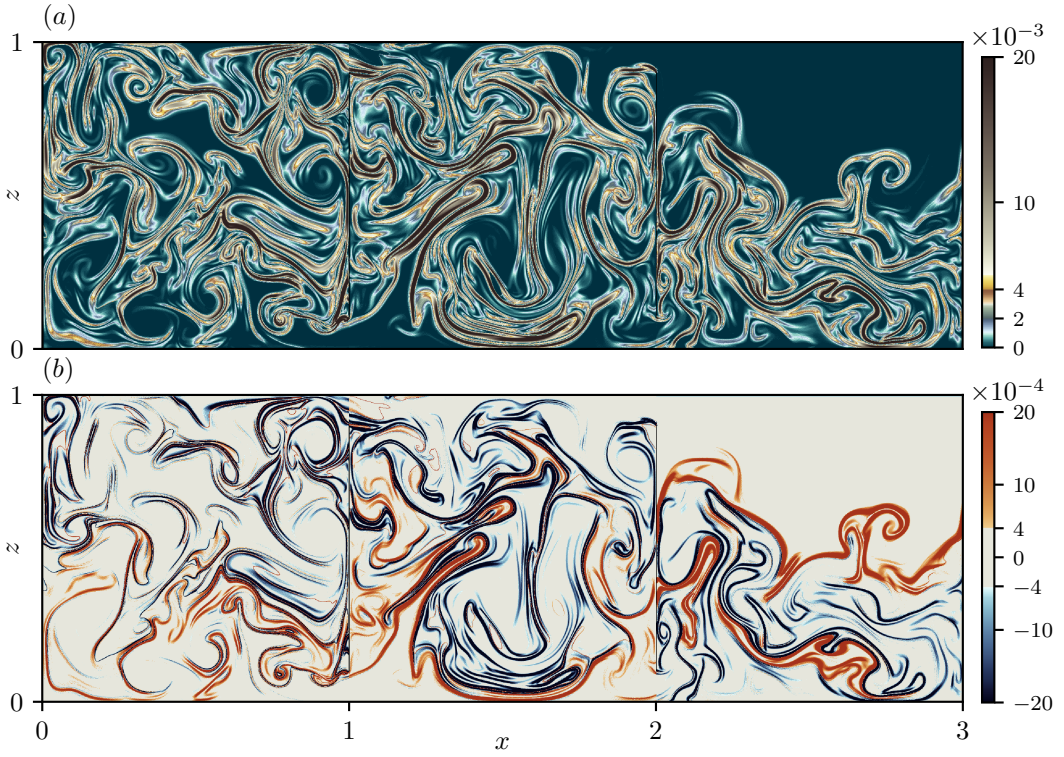


FIGURE 13. The local (pointwise) contribution to the (inner) APE dissipation $D(\omega)$ in each subvolume ω is displayed in panel (a) and the (outer) APE dissipation $D(\Omega|\omega) = D(\omega|\Omega) - D(\omega)$ is displayed in panel (b) (note the factor 10 difference in the scales used for the colormaps). The local (pointwise) contributions to $D(\omega)$ and $D(\Omega|\omega)$ can be found in equations (4.5) and (4.7), respectively. The (outer) APE dissipation $D(\Omega|\omega)$ represents a conversion between inner and outer APE (see figure 7 for reference). All variables are plotted at $t = 9.8$, after the initial condition shown in figure 4 (cf. panel (g) in figure 8). The colour map for (a) is part of the 'Outlier-Focused Colormaps' found at 'https://sciviscolor.org', which provides the 'Colormoves' interface that was used to construct the colour map in (b) (see, for example, Samsel *et al.* 2019).

and inner $A(\omega_1)$ contributions to the total APE of ω_1 relative to the reference state of the global/parent volume Ω.

Before being mixed, the fluid in ω_1 has a BPE equal to $B(\omega_1) = -1/12$, while the fluid in ω_2 has BPE $B(\omega_2) = -5/24$. A separate calculation, based on the reference state of Ω, shows that $B(\Omega) = -1/3 < -7/24 = B(\omega_1) + B(\omega_2)$, which is in accordance with the subadditive property of subvolume BPE (2.15), and indicates that (prior to mixing in ω_1) part of the background potential energy in ω_1 can be released by 'connecting' ω_1 with ω_2. When subtracted from the potential energy of ω_1 and Ω, these BPE values imply that the inner APE $A(\omega_1) = 1/8$ and $A(\Omega) = 1/6 > A(\omega_1)$, which, since $A(\omega_2) = 0$, illustrates that the buoyancy field of Ω has APE that, rather than being wholly intrinsic to ω_1, depends on the context provided by Ω. This extrinsic contribution to the global APE $A(\Omega)$ was defined as the outer APE $A(\Omega|\omega_1)$ in §2. Indeed, noting the symmetry of $2(c)$ about $z = 0$, and integrating (2.6) to find the total APE of ω_1, with knowledge of

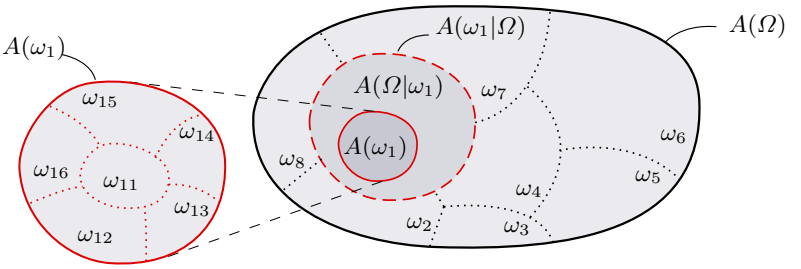


FIGURE 14. A conceptual illustration of the partitioning of a system's APE using the decomposition developed in §2 and expressed in the recursive relation (2.11). Subvolume ω_1's contribution to the global APE $A(\Omega)$ comprises inner APE $A(\omega_1)$ and outer APE $A(\Omega|\omega_1)$, which sum to give the total APE $A(\omega_1|\Omega)$ of ω_1. As shown on the left-hand side, a given subvolume ω_1 can itself be partitioned into $\omega_{11},\ldots,\omega_{16}$, which allows the decomposition to be applied recursively, as explained in §6.2.

Ω,

$$A(\omega_1|\Omega) = 2\int_{-1/2}^{0}\Bigg[\underbrace{(z+1)\left(z+\frac{1}{2}\right)}_{[z(\Omega)-z]b} - \underbrace{\int_{z}^{2z+1}\frac{\eta}{2}\,\mathrm{d}\eta}_{a_*(\Omega)}\Bigg]\,\mathrm{d}z = \frac{7}{48}, \tag{6.1}$$

which contributes to the decomposition of $A(\Omega)$ in the following way

$$A(\Omega) = \overbrace{\underbrace{A(\Omega|\omega_1)}_{1/48} + \underbrace{A(\omega_1)}_{1/8}}^{A(\omega_1|\Omega)=7/48} + \overbrace{\underbrace{A(\Omega|\omega_2)}_{1/48} + \underbrace{A(\omega_2)}_{0}}^{A(\omega_2|\Omega)=1/48} = \frac{1}{6}. \tag{6.2}$$

After mixing, which homogenises the buoyancy in ω_1 (see the thin red line in figure 2(*c*)), $B(\omega_1) = 0$, $B(\omega_2) = -5/24$ (unchanged) and, therefore, $B(\Omega) = -5/24$, which enables calculation of the following mixing efficiency over Ω:

$$\frac{\Delta B(\Omega)}{A(\Omega)} = \frac{\overbrace{\Delta B(\Omega|\omega_1)}^{1/48} + \overbrace{\Delta B(\omega_1)}^{1/12} + \overbrace{\Delta B(\Omega|\omega_2)}^{1/48} + \overbrace{\Delta B(\omega_2)}^{0}}{\underbrace{A(\Omega|\omega_1)}_{1/48} + \underbrace{A(\omega_1)}_{1/8} + \underbrace{A(\Omega|\omega_2)}_{1/48} + \underbrace{A(\omega_2)}_{0}} = \frac{3}{4}. \tag{6.3}$$

In the absence of the additional context provided by ω_2, (6.3) reduces to 2/3, which is in agreement with Davies Wykes *et al.* (2015). The context provided by Ω affects the production of BPE and initial APE, and therefore affects the numerator and denominator of (6.3), which illustrates that the composite nature of mixing efficiency makes it a difficult quantity to decompose and therefore fully understand in systems made of interconnected parts.

6.2. *Recursive properties of the decomposition*

The decomposition in (2.11) expresses the inner APE of Ω as a sum of the outer and inner APE associated with each of its constituent subvolumes. If a subvolume ω_m is partitioned into further subvolumes, then (2.11) can be applied recursively in evaluating the inner APE $A(\omega_m)$, as illustrated in figure 14.

Although subvolumes can be recursively decomposed, the inner APE associated with the smallest subvolumes tends to zero. In that case the inner APE associated with the

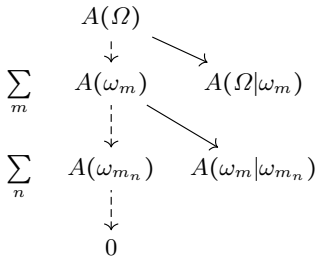


FIGURE 15. The recursive application of (2.11) to compute the global APE $A(\Omega)$ as a nested sum of outer APE contributions from exponentially smaller volumes (second column). As the volumes tend to zero, the contribution from inner APE tends to zero (first column).

root or largest parent volume Ω is obtained by summing the outer APE contributions in the second column of figure 15. For example, the individual computational cells in the simulations reported in §5 have zero inner APE because they consist of a single buoyancy. In the absence of any 'subgrid' APE in direct numerical simulation, for which $A(\omega)$ might otherwise account, the outer APE of each computational cell relative to a parent volume therefore corresponds to its local APE density (with respect to the parent volume's reference state) multiplied by its volume. The recursive application of (2.11) is therefore captured by figure 15, which could contain an arbitrary number of intermediate rows.

The decomposition described in §2 was designed for environments with clearly defined subvolumes created by physical boundaries, such as the walls and floors of buildings. However, the arguments above suggest that it might be useful in analysing the role and interaction of APE at different scales in heterogeneous environments more generally.

7. Conclusions

Inner and outer contributions to the APE of a subvolume $\omega \subset \Omega$ of a Boussinesq fluid flow have been defined, where the inner contribution accounts for the APE within ω, regardless of the parent volume Ω, and the outer contribution accounts for the APE arising from the context provided by Ω. The inner and outer components of APE are positive definite and follow naturally from previous definitions of local (pointwise) APE density. The decomposition has a clear physical interpretation, describing the potential energy that can be released within ω followed by the potential energy that can be released when the (physical or abstract) constraints that separate ω from Ω are removed.

The decomposition is useful for analysing the energetics behind systems of connected control volumes, such as rooms within buildings. There, the constraints provided by walls and floors influence the fluid mechanics and suggest convenient models comprised of networks of interconnected 'zones'. Such zonal models are efficient, used widely in industry and have an appealing simplicity, but they do not account for the 'subgrid-scale' physics of mixing within individual rooms. In particular, since air in rooms is thermally stratified, the parameterisation of mixing is important because of its influence on thermal comfort and in determining inter-zonal (or large-scale) circulation and transport. For similar reasons, the decomposition will hopefully find use in the analysis and modelling of subgrid-scale processes in the atmosphere or ocean (see, for example, Smith 1973). More generally, the approach might provide new avenues to explore in seeking physically

meaningful decompositions of local APE density into mean and eddy components (see, for example, Scotti & White 2014; Tailleux 2018).

The analysis of the budgets associated with inner and outer APE in §5.3 identified two ways in which inner APE can be converted to outer APE. The first, described in §4.2, relates to irreversible mixing and to the example shown in figure 2(b). When constraints are provided by solid boundaries, diapycnal mixing in a subvolume ω can yield outer APE by raising the centre of mass of a subvolume relative to adjacent subvolumes. The second, described in §4.3, relates to advective and diffusive transport between adjacent subvolumes. Individually, inner APE density and outer APE density are not conserved under transport between subvolumes, because they depend on the context provided by a particular subvolume and its parent, respectively. However, their sum corresponds to the total APE density, which does not account for local context and is therefore continuous across subvolumes. Consequently, transport of mass or heat between subvolumes results in a reversible conversion between inner and outer APE that accounts for the change of context without changing the total APE density.

It might be tempting to regard the inner APE for each subvolume as unavailable in the sense that it does not appear to be directly responsible for driving large-scale flow between subvolumes. However, the possibility of conversion between inner and outer APE identified in §4.3, and described in the previous paragraph, makes the situation more subtle. In a given case one should expect the eventual roles played by inner and outer APE in driving circulation between sub volumes to depend crucially on the various competing time scales involved.

The coupling between inner and outer APE with the kinetic energy budget is an area that would benefit from further research. In this regard, the kinetic energy could be decomposed into inner (subgrid-scale) and outer (large-scale) components. For example, the conversion term $C(\Omega|\omega)$ in the outer APE budget (4.7) is likely to appear with an opposite sign in any budget that focuses on the kinetic energy associated with the mean motion within and between subvolumes. In contrast, $C(\omega)$ in the inner APE budget (4.5) accounts for conversion between APE and kinetic energy within a subvolume that is notionally assumed to be closed.

Acknowledgements. The author would like to thank Rémi Tailleux, Graham O. Hughes and anonymous reviewers for providing helpful suggestions.

Declaration of Interests. The author reports no conflict of interest.

Appendix A. Formulae for analytical example

Table 1 provides analytical expressions for the APE decomposition presented in figure 6 based on the initial conditions depicted in figure 4. The table focuses on cases in which $0 \leqslant b_1 \leqslant b_2 \leqslant 1$ and $b_1 = 1$, $b_2 = 0$. Different configurations of buoyancy, which would change the global reference state shown on the right-hand side of figure 4, would produce different expressions, demarcated by the gradient discontinuities in figure 6(b).

REFERENCES

Andrews, D. G. 1981 A note on potential energy density in a stratified compressible fluid. *Journal of Fluid Mechanics* **107**, 227–236.

Andrews, D. G. 2006 On the available energy density for axisymmetric motions of a compressible stratified fluid. *Journal of Fluid Mechanics* **569**, 481–492.

		$0 \leqslant b_1 \leqslant b_2 \leqslant 1$	$b_1 = 1,\ b_2 = 0$
	$A(\Omega)$	$\frac{L}{8}\left(\lambda(1-\lambda)+\lambda(\lambda+4\mu-1)b_1+4\mu\nu b_2\right)+\sum_n A(\omega_n)$	$\frac{L}{2}\lambda(1-\lambda)$
	$A(\Omega\,\vert\,\omega_1\cup\omega_2)$	$A(\Omega)-A(\Omega\vert\omega_3)-A(\omega_3)-A(\omega_1\cup\omega_2)$	$\frac{L}{2}\frac{\lambda^2\nu^2}{1-\nu}$
	$A(\Omega\,\vert\,\omega_2\cup\omega_3)$	$A(\Omega)-A(\Omega\vert\omega_1)-A(\omega_1)-A(\omega_2\cup\omega_3)$	$\frac{L}{2}\lambda^2(1-\lambda)$
*	$A(\Omega\,\vert\,\omega_3\cup\omega_1)$	$A(\Omega)-A(\Omega\vert\omega_2)-A(\omega_2)-A(\omega_3\cup\omega_1)$	$\frac{L}{2}\frac{\lambda^2\mu^2}{1-\mu}$
	$A(\omega_1\cup\omega_2)$	$\frac{L}{8}\frac{\lambda\mu}{1-\nu}(1+3b_1)+A(\omega_1)$	$\frac{L}{2}\frac{\lambda\mu}{1-\nu}$
	$A(\omega_2\cup\omega_3)$	$\frac{L}{2}\frac{\mu\nu}{1-\lambda}b_2$	0
*	$A(\omega_3\cup\omega_1)$	$\frac{L}{8}\left(3\lambda-\frac{\lambda^2}{1-\mu}\right)(1-b_1)$	$\frac{L}{2}\frac{\nu\lambda}{1-\mu}$
	$A(\omega_1\cup\omega_2\,\vert\,\omega_1)$	$A(\omega_1\cup\omega_2)-A(\omega_1\cup\omega_2\vert\omega_2)-\sum_{n\neq 3}A(\omega_n)$	$\frac{L}{2}\frac{\lambda\mu^2}{(1-\nu)^2}$
	$A(\omega_1\cup\omega_2\,\vert\,\omega_2)$	$\frac{L}{8}\frac{\lambda^2\mu}{(1-\nu)^2}(1+3b_1)$	$\frac{L}{2}\frac{\lambda^2\mu}{(1-\nu)^2}$
	$A(\omega_2\cup\omega_3\,\vert\,\omega_3)$	$A(\omega_2\cup\omega_3)-A(\omega_2\cup\omega_3\vert\omega_2)-\sum_{n\neq 1}A(\omega_n)$	0

TABLE 1. (Continued on the next page). Inner and outer contributions to APE based on the initial conditions depicted in figure 4 and presented in figure 6. The entries marked '*' correspond to volumes that are not spatially adjacent (see figure 5) but are included here for completeness and to aid calculation.

AXLEY, J. 2007 Multizone airflow modeling in buildings: History and theory. *HVAC&R Research* **13** (6), 907–928.

BHAGAT, R. K., DAVIES WYKES, M. S., DALZIEL, S. B. & LINDEN, P. F. 2020 Effects of ventilation on the indoor spread of COVID-19. *Journal of Fluid Mechanics* **903**, F1.

CAULFIELD, C. P. 2020 Open questions in turbulent stratified mixing: Do we even know what we do not know? *Phys. Rev. Fluids* **5**, 110518.

CRASKE, J. & HUGHES, G. 2019 On the robustness of emptying filling boxes to sudden changes in the wind. *Journal of Fluid Mechanics* **868**, R3.

CRASKE, J. & VAN REEUWIJK, M. 2015 Energy dispersion in turbulent jets. Part 1. Direct simulation of steady and unsteady jets. *Journal of Fluid Mechanics* **763**, 500–537.

DAVIES WYKES, M. S., HOGG, C., PARTRIDGE, J. & HUGHES, G. O. 2019 Energetics of mixing for the filling box and the emptying-filling box. *Environmental Fluid Mechanics* **19**, 819–831.

DAVIES WYKES, M. S., HUGHES, G. O. & DALZIEL, S. B. 2015 On the meaning of mixing efficiency for buoyancy-driven mixing in stratified turbulent flows. *Journal of Fluid Mechanics* **781**, 261–275.

DEWAR, W. K. & MCWILLIAMS, J. C. 2019 On energy and turbulent mixing in the thermocline. *Journal of Advances in Modeling Earth Systems* **11** (3), 578–596.

FERNANDO, H. J. S. 1991 Turbulent mixing in stratified fluids. *Annual Review of Fluid Mechanics* **23** (1), 455–493.

GAGGIOLI, R. 1998 Available energy and exergy. *International Journal of Thermodynamics* .

HAYWOOD, R. W. 1974 A critical review of the theorems of thermodynamic availability, with concise formulations. *Journal of Mechanical Engineering Science* **16** (4), 258–267.

		$0 \leqslant b_1 \leqslant b_2 \leqslant 1$	$b_1 = 1,\ b_2 = 0$
	$A(\omega_2 \cup \omega_3 \,\vert\, \omega_2)$	$\frac{L}{2}\frac{\mu\nu^2}{(1-\lambda)^2}b_2$	0
*	$A(\omega_3 \cup \omega_1 \,\vert\, \omega_1)$	$A(\omega_3 \cup \omega_1) - A(\omega_3 \cup \omega_1 \vert \omega_3) - \sum_{n\neq 2} A(\omega_n)$	$\frac{L}{2}\frac{\nu^2\lambda}{(1-\mu)^2}$
*	$A(\omega_3 \cup \omega_1 \,\vert\, \omega_3)$	$\frac{L}{8}\frac{\nu\lambda^2}{(1-\mu)^2}(1-b_1)$	$\frac{L}{2}\frac{\nu\lambda^2}{(1-\mu)^2}$
	$A(\Omega \,\vert\, \omega_1)$	$A(\Omega) - A(\Omega \vert \omega_3) - A(\Omega \vert \omega_2) - \sum_n A(\omega_n)$	$\frac{L}{2}\lambda(1-\lambda)^2$
	$A(\Omega \,\vert\, \omega_2)$	$\frac{L}{8}\mu\left(\lambda^2 + \lambda(3\lambda+4\nu)b_1 + 4\nu(1-\mu)b_2\right)$	$\frac{L}{2}\lambda^2\mu$
	$A(\Omega \,\vert\, \omega_3)$	$\frac{L}{8}\nu\left(\lambda^2 - \lambda(\lambda+4\mu)b_1 + 4\mu(1-\nu)b_2\right)$	$\frac{L}{2}\lambda^2\nu$
	$A(\omega_1)$	$\frac{L}{4}\lambda(1-b_1)$	0
	$A(\omega_2)$	0	0
	$A(\omega_3)$	0	0

TABLE 1. (Continued from the previous page).

HOLLIDAY, D. & MCINTYRE, M. E. 1981 On potential energy density in an incompressible, stratified fluid. *Journal of Fluid Mechanics* **107**, 221–225.

IVEY, G., WINTERS, K. & KOSEFF, J. 2008 Density stratification, turbulence, but how much mixing? *Annual Review of Fluid Mechanics* **40** (1), 169–184.

KANG, D. & FRINGER, O. 2010 On the Calculation of Available Potential Energy in Internal Wave Fields. *Journal of Physical Oceanography* **40** (11), 2539–2545.

KEENAN, J. H. 1951 Availability and irreversibility in thermodynamics. *British Journal of Applied Physics* **2** (7), 183–192.

KUCHARSKI, F. 1997 On the concept of exergy and available potential energy. *Quarterly Journal of the Royal Meteorological Society* **123** (543), 2141–2156.

KUESTERS, A. S. & WOODS, A. W. 2012 On the competition between lateral convection and upward displacement in a multi-zone naturally ventilated space. *Journal of Fluid Mechanics* **707**, 393–404.

LAMB, K. 2008 On the calculation of the available potential energy of an isolated perturbation in a density-stratified fluid. *Journal of Fluid Mechanics* **597**, 415–427.

LINDEN, P. F. 1979 Mixing in stratified fluids. *Geophysical & Astrophysical Fluid Dynamics* **13** (1), 3–23.

LINDEN, P. F. 1999 The fluid mechanics of natural ventilation. *Annual Review of Fluid Mechanics* **31** (1), 201–238.

LITTLEJOHN, R. G. 1982 Singular Poisson tensors. *AIP Conference Proceedings* **88** (1), 47–66.

LORENZ, E. 1955 Available potential energy and the maintenance of the general circulation. *Tellus* **7** (2), 157–167.

MACLANE, S. & BIRKHOFF, G. 1999 *Algebra*. Chelsea Publishing Company.

MARGULES, M. 1903 Über die Energie der Stürme. *Jahrb. Zent.-Anst. für Meteorol. und Erdmagnet.* **48**, 1–26.

PELTIER, W. R. & CAULFIELD, C. P. 2003 Mixing efficiency in stratified shear flows. *Annual Review of Fluid Mechanics* **35** (1), 135–167.

Roullet, G. & Klein, P. 2009 Available potential energy diagnosis in a direct numerical simulation of rotating stratified turbulence. *Journal of Fluid Mechanics* **624**, 45–55.

Samsel, F., Wolfram, P., Bares, A., Turton, T. L. & Bujack, R. 2019 Colormapping resources and strategies for organized intuitive environmental visualization. *Environmental Earth Sciences* **78** (269).

Scotti, A., Beardsley, R. & Butman, B. 2006 On the interpretation of energy and energy fluxes of nonlinear internal waves: an example from Massachusetts Bay. *Journal of Fluid Mechanics* **561**, 103–112.

Scotti, A. & Passaggia, P.-Y. 2019 Diagnosing diabatic effects on the available energy of stratified flows in inertial and non-inertial frames. *Journal of Fluid Mechanics* **861**, 608–642.

Scotti, A. & White, B. 2014 Diagnosing mixing in stratified turbulent flows with a locally defined available potential energy. *Journal of Fluid Mechanics* **740**, 114–135.

Shepherd, T. G. 1993 A unified theory of available potential energy. *Atmosphere-Ocean* **31** (1), 1–26.

Smith, P. J. 1973 The Net Generation of Large-Scale Available Potential Energy by Subgrid-Scale Processes. *Journal of the Atmospheric Sciences* **30** (8), 1714–1717.

Smith, R. K., Montgomery, M. T. & Zhu, H. 2005 Buoyancy in tropical cyclones and other rapidly rotating atmospheric vortices. *Dynamics of Atmospheres and Oceans* **40** (3), 189–208.

Stewart, K., Saenz, J. A., Hogg, A. M., Hughes, G. O. & Griffiths, R. W. 2014 Effect of topographic barriers on the rates of available potential energy conversion of the oceans. *Ocean Modelling* **76**, 31–42.

Tailleux, R. 2009 On the energetics of stratified turbulent mixing, irreversible thermodynamics, Boussinesq models and the ocean heat engine controversy. *Journal of Fluid Mechanics* **638**, 339–382.

Tailleux, R. 2013*a* Available potential energy and exergy in stratified fluids. *Annual Review of Fluid Mechanics* **45** (1), 35–58.

Tailleux, R. 2013*b* Available potential energy density for a multicomponent Boussinesq fluid with arbitrary nonlinear equation of state. *Journal of Fluid Mechanics* **735**, 499–518.

Tailleux, R. 2018 Local available energetics of multicomponent compressible stratified fluids. *Journal of Fluid Mechanics* **842**, R1.

Thorpe, S. A. 1977 Turbulence and mixing in a Scottish Loch. *Philosophical Transactions of the Royal Society of London. Series A, Mathematical and Physical Sciences* **286** (1334), 125–181.

Tseng, Y. & Ferziger, J. H. 2001 Mixing and available potential energy in stratified flows. *Physics of Fluids* **13** (5), 1281–1293.

Van Mieghem, J. 1956 The energy available in the atmosphere for conversion into kinetic energy. *Beiträge Zur Physik der Atmosphäre* **29** (2), 129–142.

Weinstein, A. 1983 The local structure of Poisson manifolds. *J. Differential Geom.* **18** (3), 523–557.

Winters, K. B. & Barkan, R. 2013 Available potential energy density for Boussinesq fluid flow. *Journal of Fluid Mechanics* **714**, 476–488.

Winters, K. B., Lombard, P. N., Riley, J. J. & D'Asaro, E. A. 1995 Available potential energy and mixing in density-stratified fluids. *Journal of Fluid Mechanics* **289**, 115–128.